The decomposition of the higher-order homology embedding constructed from the k-Laplacian

Yu-Chia Chen
Electrical & Computer Engineering
University of Washington
Seattle, WA 98195
yuchaz@uw.edu

Marina Meilă
Department of Statistics
University of Washington
Seattle, WA 98195
mmp2@uw.edu

Abstract

The null space of the k-th order Laplacian $\mathcal{L}_k$, known as the *k-th homology vector space*, encodes the non-trivial topology of a manifold or a network. Understanding the structure of the homology embedding can thus disclose geometric or topological information from the data. The study of the null space embedding of the graph Laplacian $\mathcal{L}_0$ has spurred new research and applications, such as spectral clustering algorithms with theoretical guarantees and estimators of the Stochastic Block Model. In this work, we investigate the geometry of the k-th homology embedding and focus on cases reminiscent of spectral clustering. Namely, we analyze the *connected sum* of manifolds as a perturbation of the direct sum of their homology embeddings. We propose an algorithm to factorize the homology embedding into subspaces corresponding to a manifold's simplest topological components. The proposed framework is applied to the *shortest homologous loop detection* problem, a problem known to be NP-hard in general. Our spectral loop detection algorithm complements existing methods of topological data analysis. It scales better than existing methods with no assumptions on the structure of data and is effective on diverse data such as point clouds and images.

1 Motivation

The k-th *homology vector space* $\mathcal{H}_k$ provides rich geometric information on manifolds/networks. For instance, the zeroth, the first, and the second homology vector spaces identify the connected components, the loops, and the cavities in the manifold, respectively. Topological Data Analysis (TDA) [24, 58] (as well as other early works in this field) has found wide use in analyzing biological [31, 47], human behavior [1, 64], or other complex systems [58]. Even though they easily generalize to $k \geq 1$, additional efforts are needed to extract topological features (e.g., instances of loops) besides ranks due to the combinatorial complexity of the structures that support them.

Spectral methods based on k-Laplacians ($\mathcal{L}_k$), by contrast, investigate $\mathcal{H}_k$ in a linear algebraic manner; abundant geometric information can be extracted from the *homology embedding* $\mathbf{Y}$ (the null space eigenvectors of $\mathcal{L}_k$) of $\mathcal{H}_k$. Analysis of the eigenfunctions (of $\mathcal{H}_0$) [14, 37, 40, 49] of the graph Laplacian $\mathcal{L}_0$ is pivotal in providing guarantees for spectral clustering and community detection algorithms in well-separated datasets. Recent advances in this field [4, 12, 48] extend the existing spectral algorithms based on $\mathcal{L}_0$ to $k \geq 1$; however, the theoretical analysis of $\mathbf{Y}$ of $\mathcal{H}_k$, unlike spectral clustering, is less developed, in spite of intriguing empirical results by [21]. Here, we put these observations on a formal footing based on the concepts of *connected sum* and *prime decomposition* of manifolds (Section 2 and 3). We examine these operations through the lens of the (subspace) perturbation to the homology embedding $\mathbf{Y}$ of the discrete k-Laplacian $\mathcal{L}_k$ (an estimator of the continuous k-Hodge Laplacian operator Δ_k) on finite samples (Section 4). This framework

35th Conference on Neural Information Processing Systems (NeurIPS 2021).

finds applications in, i.e., identifying the *shortest homologous loops* (Section 5). Lastly, we support our theoretical claims with numerous empirical results from point clouds and images.

2 Background in Hodge theory and topology

Simplicial and cubical complex. An *abstract complex* is a natural extension of a graph designed to capture higher-order relationships between its vertices. A *simplicial k-complex* (used when the data are point clouds or networks) is a tuple $\mathrm{SC}_k = (\Sigma_0, \cdots, \Sigma_k)$, with Σ_ℓ being a set of ℓ dimensional *simplices*, such that every *face* of a simplex $\sigma \in \Sigma_\ell$ is in $\Sigma_{\ell-1}$ for $\ell \leq k$. As a side note, a graph $G = (V, E)$ is an SC_1; and $\mathrm{SC}_2 = (V, E, T)$, which is commonly used in edge flow learning [12, 48], is obtained by adding a set of 3-cliques (triangles) T of G. This procedure extends to defining Σ_ℓ as the set of all ℓ-cliques of G, with the resulting complex called a *clique complex* of the graph G. This complex is also known as a *Vietoris-Rips (VR) complex* if G is the ϵ-radius neighborhood graph used in the manifold learning literature [12, 14, 53], The *cubical k-complex* $\mathrm{CB}_k = (K_0, \cdots, K_k)$ is a complex widely used with image data. The difference between this complex and the SC_k is that a CB_k is a collection of sets of ℓ-cubes, for $\ell < k$. Note that we write $\Sigma_0 = K_0 = V$ the vertex set and $\Sigma_1 = K_1 = E$ the edge set. $\Sigma_2 = T$ and $K_2 = R$ are the triangle and rectangle set, respectively. Additionally, we define $n_\ell = |\Sigma_\ell|$ (or $= |K_\ell|$) to be the cardinality of the ℓ-dimensional cells and let $n = n_0$ for simplicity. For more information about building various complexes on different datasets please refer to Otter et al. [43].

k-cochain. By choosing an orientation for every k-simplex $\sigma_{k,i} \in \Sigma_k$ (or K_k), one can define a finite-dimensional vector space $\mathcal{C}_k$ (k-*cochain space*[1]). An element $\boldsymbol{\omega}_k = \sum_i \boldsymbol{\omega}_k(\sigma_{k,i})\sigma_{k,i} \in \mathcal{C}_k$ is called a k-*cochain*; one can further express $\boldsymbol{\omega}_k$ as $\boldsymbol{\omega}_k = (\omega_{k,1}, \cdots, \omega_{k,n_k})^\top \in \mathbb{R}^{n_k}$ by identifying each $\sigma_{k,i}$ with the standard basis vector $\mathbf{e}_i \in \mathbb{R}^{n_k}$. Functions on nodes and edge flows, for example, are elements of $\mathcal{C}_0$ and $\mathcal{C}_1$, respectively.

Boundary matrix. The k-th *boundary matrix* $\mathbf{B}_k$ [35] maps a k-cochain of k-cells (simplices/cubes) σ_k to the $(k-1)$-cochain of its faces, i.e., $\mathbf{B}_k : \mathcal{C}_k \to \mathcal{C}_{k-1}$. $\mathbf{B}_k \in \{0, \pm 1\}^{n_{k-1} \times n_k}$ is a sparse binary matrix, with the sign of the non-zero entries σ_{k-1}, σ_k given by the orientation of σ_k w.r.t. its face σ_{k-1}. Hence, different SC or CB will induce different $\mathbf{B}_k$. For $k = 1$ on either the SC or CB, the boundary map is the *graph incidence matrix*, i.e., $(\mathbf{B}_1)_{[x],[x,y]} = 1$, $(\mathbf{B}_1)_{[y],[x,y]} = -1$, and zero otherwise; for $k = 2$, each column of $\mathbf{B}_2$ contains the orientation of a triangle/rectangle w.r.t. its edges. Specifically, for an SC, $(\mathbf{B}_2)_{[x,y],[x,y,z]} = (\mathbf{B}_2)_{[y,z],[x,y,z]} = 1$, $(\mathbf{B}_2)_{[x,z],[x,y,z]} = -1$, and 0 otherwise; for a CB, $(\mathbf{B}_2)_{[x,y],[x,y,z,w]} = (\mathbf{B}_2)_{[y,z],[x,y,z,w]} = (\mathbf{B}_2)_{[z,w],[x,y,z,w]} = 1$, $(\mathbf{B}_2)_{[x,w],[x,y,z,w]} = -1$, and 0 otherwise. Simplex σ_{k+1} is a *coface* of σ_k iff σ_k is a face of σ_{k+1}; let $\mathrm{coface}(\sigma_k)$ be the set of all cofaces of σ_k. The $(k-1)$-th *coboundary matrix* $\mathbf{B}_k^\top$ (adjoint of $\mathbf{B}_k$) maps σ_{k-1}, as a $(k-1)$-cochain, to the k-cochain of $\mathrm{coface}(\sigma_{k-1})$.

k-Hodge Laplacian. Let $\mathbf{W}_\ell$ be a diagonal non-negative *weight matrix* of dimension n_ℓ, with $[\mathbf{W}_\ell]_{\sigma,\sigma}$ representing the weight of the ℓ-simplex/cube σ and $\mathbf{w}_\ell \leftarrow \mathrm{diag}(\mathbf{W}_\ell)$. The weighted k-Hodge Laplacian[2] [26] is defined as

$$\boldsymbol{\mathcal{L}}_k = \mathbf{A}_k^\top \mathbf{A}_k + \mathbf{A}_{k+1}\mathbf{A}_{k+1}^\top, \ \ \text{where} \ \ \mathbf{A}_\ell = \mathbf{W}_{\ell-1}^{-1/2}\mathbf{B}_\ell \mathbf{W}_\ell^{1/2} \ \text{for} \ \ell = k, k+1. \quad (1)$$

The weights capture combinatorial or geometric information and must satisfy the consistency relation $\mathbf{w}_\ell(\sigma_\ell) = \sum_{\sigma_{\ell+1} \in \mathrm{coface}(\sigma_\ell)} \mathbf{w}_{\ell+1}(\sigma_{\ell+1})$ (in matrix form: $\mathbf{w}_\ell = |\mathbf{B}_{\ell+1}|\mathbf{w}_{\ell+1}$) for $\ell = k, k-1$. Hence $\mathbf{A}_k$ can be seen as normalized boundary matrix. To determine the weight for the $(k+1)$-simplices, one can selected $\mathbf{w}_{k+1}$ to be constant [48] or based on (a product of) pairwise distance kernel (for $k = 0, 1$) so that the large sample limit exists [12, 14]. The first and second terms of (1) are called respectively the *down* ($\boldsymbol{\mathcal{L}}_k^{\mathrm{down}} = \mathbf{A}_k^\top \mathbf{A}_k$) and *up* ($\boldsymbol{\mathcal{L}}_k^{\mathrm{up}} = \mathbf{A}_{k+1}\mathbf{A}_{k+1}^\top$) Laplacians. For $k = 0$, the down component disappears and the resulting $\boldsymbol{\mathcal{L}}_0$ is the *symmetric normalized* graph Laplacian used in spectral clustering [55] and Laplacian Eigenmap [5].

---

[1]We use *chain* and *cochain* interchangeably, see Lim [35] for the distinction between them.
[2]In this paper, these matrices are also called the k-Laplacian for simplicity.

2

k-th homology vector space and embedding. The homology vector space $\mathcal{H}_k$ is a subspace of $\mathcal{C}_k$ (loop space) such that every k-cycle (expressed as a k-cochain) in $\mathcal{H}_k$ is not the boundary of any $(k+1)$-cochain. In mathematical terms, $\mathcal{H}_k := \ker(\mathbf{A}_k)/\mathrm{im}(\mathbf{A}_{k+1})$. The rank of the subspace is called the k-th Betti number $\beta_k = \dim(\mathcal{H}_k)$, which counts the number of "loops" (*homology classes*) in the SC. $\mathcal{H}_k$ is equivalent to the null space of $\mathcal{L}_k$ [35, 48]; therefore, a basis of $\mathcal{H}_k$ can be obtained by the eigenvectors $\mathbf{Y} = [\mathbf{y}_1, \cdots, \mathbf{y}_{\beta_k}] \in \mathbb{R}^{n_k \times \beta_k}$ of $\mathcal{L}_k$ with eigenvalue 0. The *homology embedding* maps a k-simplex σ_k to $\mathbf{Y}_{\sigma_k,:} = [\mathbf{y}_1(\sigma_k), \cdots \mathbf{y}_{\beta_k}(\sigma_k)]^\top \in \mathbb{R}^{\beta_k}$. Note that the basis $\mathbf{Y}$ is only identifiable up to a unitary transformation; hence, individual homology embedding coordinates might change with a different basis $\mathbf{Y}$.

Continuous operators on manifolds. The k-cochains are the discrete analogues of k-*forms* [59]. For $k = 1$, the following path integral [59] (along the geodesic $\boldsymbol{\gamma}(t)$ connecting x and y) relates a 1-cochain $\boldsymbol{\omega}$ to a 1-form $\mathbf{v}$ (vector field): $\boldsymbol{\omega}([x,y]) = \int_x^y \mathbf{v}(\boldsymbol{\gamma}(t))\boldsymbol{\gamma}'(t)\mathrm{d}t$. To estimate a vector field from $\boldsymbol{\omega}$, one can solve a least-squares problem [12], which is the inverse operation of the path integral (e.g., the vector fields in Figure 1 are estimated from $\mathbf{Y}$). Similarly, one can define the *differential* d and *codifferential* δ operators which are analog to $\mathbf{B}_{k+1}^\top$ and $\mathbf{B}_k$, respectively. The (continuous) k-Hodge Laplacian operators, which act on k-forms, can be defined for manifolds too, i.e., by $\Delta_k = \mathrm{d}_{k-1}\delta_k + \delta_{k+1}\mathrm{d}_k$. The homology group (the continuous version of $\mathcal{H}_k$) is defined as the null of Δ_k. Its elements are harmonic k-forms ζ_k, computed by solving $\Delta_k\zeta_k = 0$ with proper boundary conditions; they represent the continuous version of the discrete homology basis $\mathbf{Y}$.

Connected sum and manifold (prime) decomposition. The connected sum [33] of two d dimensional manifolds $\mathcal{M} = \mathcal{M}_1 \sharp \mathcal{M}_2$ is built from removing two d dimensional "disks" from each manifold $\mathcal{M}_1$, $\mathcal{M}_2$ and gluing together two manifolds at the boundaries (technical details in [33]). The analog of the connected sum for the abstract complexes will be defined in Section 3. The connected sum is a core operation in topology and is related to the concept of manifold (prime) decomposition. Informally speaking, the prime decomposition aims to factorize a manifold $\mathcal{M}$ into κ smaller building blocks ($\mathcal{M} = \mathcal{M}_1 \sharp \cdots \sharp \mathcal{M}_\kappa$) so that each $\mathcal{M}_i$ cannot be further expressed as a connected sum of other manifolds. The well-known *classification theorem of surfaces* [3] states that any oriented and compact surface is the finite connected sum of manifolds homeomorphic to either a circle $\mathbb{S}^1$, a sphere $\mathbb{S}^2$, or a torus $\mathbb{T}^2$. Classification theorems for $d > 2$ are currently unknown; fortunately, the uniqueness of the prime decomposition for $d = 3$ (up to homeomorphism) was shown (Kneser-Milnor theorem [39]). Recently, Bokor et al. [9] (Corollary 2.5) showed the existence of factorizations of manifolds with $d \geq 5$, even though they might not be unique.

In this paper, we are interested in the following: given finite samples from $\mathcal{M}$, which is a κ-fold connected sum of $\mathcal{M}_i$, can this decomposition be recovered from the discrete homology embedding $\mathbf{Y}$ of $\mathcal{M}$? Namely, we would like to understand how $\mathbf{Y}$ relates to the homology embedding of each prime manifold $\mathcal{M}_i$.

3 Definitions, theoretical/algorithmic aims, and prior works

Definitions. We assume that the data $\mathbf{X}$ is sampled from a d-dimensional *oriented* manifold $\mathcal{M}$ that can be decomposed into κ prime manifolds ($\mathcal{M} = \mathcal{M}_1 \sharp \cdots \sharp \mathcal{M}_\kappa$). Let $\mathcal{I}_i$ be an index set of the data points in $\mathbf{X}$ sampled from $\mathcal{M}_i$, for $i = 1, \ldots \kappa$. Denote by SC_k, $\mathcal{L}_k$, $\mathcal{H}_k(\mathcal{M})$, and β_k the simplicial complex, the k-Laplacian, the k-homology space, and the k-th Betti number of $\mathbf{X}$ sampled from $\mathcal{M}$. Furthermore, let $\widehat{\mathrm{SC}}_k^{(i)} = (\widehat{\Sigma}_0^{(i)}, \cdots, \widehat{\Sigma}_k^{(i)}), \widehat{\mathcal{L}}_k^{(ii)}, \mathcal{H}_k(\mathcal{M}_i), \beta_k(\mathcal{M}_i)$ be the same quantities for manifold $\mathcal{M}_i$ (supported on $\mathcal{I}_i$ for $i \leq \kappa$). $\widehat{\mathrm{SC}}_k$ and $\widehat{\mathcal{L}}_k$ (without superscript i) are the comparable notations for the disjoint manifolds $\mathcal{M}_i$'s, i.e. $\widehat{\mathrm{SC}} = \cup_{i=1}^\kappa \widehat{\mathrm{SC}}^{(i)} = (\widehat{\Sigma}_0, \cdots, \widehat{\Sigma}_k)$ with $\widehat{\Sigma}_\ell = \cup_{i=1}^\kappa \widehat{\Sigma}_\ell^{(i)}$ for $\ell \leq k$, and $\widehat{\mathcal{L}}_k$ is a block diagonal matrix with the i-th block being $\widehat{\mathcal{L}}_k^{(ii)}$. Additionally, let $\mathbf{Y}$ and $\widehat{\mathbf{Y}}$ (both in $\mathbb{R}^{n_k \times \beta_k}$) be the homology basis of $\mathcal{L}_k$ and $\widehat{\mathcal{L}}_k$, respectively. Let $\mathcal{S}_i$ be the index set of columns of $\widehat{\mathbf{Y}}$ corresponding to homology subspace $\mathcal{H}_k(\mathcal{M}_i)$, with $\mathcal{S}_i \cap \mathcal{S}_j = \emptyset$ for $i \neq j$, $|\mathcal{S}_i| = \beta_k(\mathcal{M}_i)$, and $\mathcal{S}_1 \cup \cdots \cup \mathcal{S}_\kappa = \{1, \cdots, \beta_k\}$. Since $\widehat{\mathbf{Y}}$ is the homology embedding of a block diagonal matrix $\widehat{\mathcal{L}}_k$, we choose it so that $[\widehat{\mathbf{Y}}]_{\sigma,m}$ equals the homology embedding of $\widehat{\mathcal{L}}_k^{(ii)}$ if

3

$\sigma \in \widehat{\Sigma}_k^{(i)}$ with column $m \in \mathcal{S}_i$ and is zero otherwise. Namely, $\widehat{\mathbf{Y}}$ lies in the direct sum of subspaces $\mathcal{H}_k(\widehat{\mathcal{M}}_i)$ for $i \leq \kappa$.

Theoretical aim. We are interested in the geometric properties of the null space eigenvectors $\mathbf{Y}$, and specifically in recovering the homology basis $\widehat{\mathbf{Y}}$ of the prime manifolds. Hence, we aim to bound the *distance* between the spaces spanned by $\mathbf{Y}$ and $\widehat{\mathbf{Y}}$. Under a small perturbation, one can provide an analogous argument to the *orthogonal cone* structure [40, 49] in spectral clustering (the zeroth homology embedding). The main technical challenge is that the connected sum of manifolds is a highly localized perturbation; namely, most cells are not affected at all, while those involved in the gluing process gain or lose $\mathcal{O}(1)$ (co)faces. Without properly designing $\mathcal{L}_k$ and $\widehat{\mathcal{L}}_k$, one might get a trivial bound.

Algorithmic aim. We exemplify the algorithmic aim using $k = 1$, $d = 2$, and $\kappa = 2$, particularly the genus-2 surface shown in Figure 1. The null space basis $\mathbf{Y}$ of $\mathcal{L}_k$ is only identifiable up to a unitary matrix due to the multiplicity of the zero eigenvalues. For instance, the top and bottom rows of Figure 1 are both valid bases for the harmonic edge flows in $\mathcal{H}_1$. However, the basis vector fields in the second row of Figure 1 are more inter-

Figure 1: Harmonic vector fields obtained by solving a least-squares [12] with $\mathbf{Y}$ (top) and $\mathbf{Z}$ (bottom).

pretable than those in the top row because $\mathbf{Y}$ (the first row) is a linear combination of $\mathbf{Z}$ (the second row), with each basis (column in the figure) corresponding to a single homology class (loop). Therefore, here we propose a *data-driven* approach to obtain the optimal basis $\mathbf{Z}$ such that the coupling from other manifolds/subspaces is as weak as possible. Being able to obtain $\mathbf{Z}$ from an arbitrary $\mathbf{Y}$ can support numerous applications (more in Section 5); however, it is difficult to design a criterion for finding the optimal $\mathbf{Z}$ without knowing the geometric structure of the embedding of $\mathcal{H}_k$.

Prior work. The shape of the embedding by the principal eigenvectors of the graph Laplacian $\mathcal{L}_0$ is pivotal for showing the guarantees of spectral clustering algorithms for point cloud data or the inference algorithms for the stochastic block model. The analyses used either the matrix perturbation theory [40, 55, 56] or assume a mixture model [49]. For the higher-order k-Laplacian, it is reported empirically that the homology embedding is approximately distributed on the union (directed sum) of subspaces [21]; subspace clustering algorithms [30] were applied to partition edges/triangles under their framework.

On the application side, the eigen-embedding of $\mathcal{L}_k$ is used implicitly or explicitly in graph signal processing [27, 44, 45] and in learning algorithms utilizing Hodge decomposition [12, 28, 62]. They use the gradient/curl cochains (which correspond to the images of $\mathcal{L}_k^{\mathrm{down}}$ and $\mathcal{L}_k^{\mathrm{up}}$, respectively) in addition to the homology embedding ($\ker(\mathcal{L}_k)$); hence, our framework is intrinsically different from these works.

4 Main result: connected sum as a matrix perturbation

In this section, we analyze the geometric structure of $\mathbf{Y}$ by viewing the operation of *connected sum* through the lens of matrix perturbation theory [51]. We show that, under certain conditions, the homology embedding $\mathbf{Y}$ of the joint Laplacian $\mathcal{L}_k$ is approximated by $\widehat{\mathbf{Y}}$ for the simplices in $\Sigma_k \cap \widehat{\Sigma}_k$. In matrix terms, we show that $\mathbf{Y} \approx \widehat{\mathbf{Y}}\mathbf{O}$ (Theorem 1) with $\mathbf{O}$ a unitary transformation.

We first prepare our assumptions suited for SC built from point clouds. Most of the assumptions (except Assumption 1 for which the connected sum might not be defined) can be extended to the clique complex (for networks) or cubical complex (for images) without too many modifications.

Assumption 1. *The point cloud $\mathbf{X} \in \mathbb{R}^{n \times D}$ is sampled from a d-dimensional oriented and compact manifold $\mathcal{M} \subseteq \mathbb{R}^D$; the homology vector spaces $\mathcal{H}_k(\mathrm{SC})$ formed by the simplicial complex constructed from $\mathbf{X}$ are isomorphic to the homology group $\mathcal{H}_k(\mathcal{M})$ of $\mathcal{M}$, i.e., $\mathcal{H}_k(\mathrm{SC}) \simeq \mathcal{H}_k(\mathcal{M})$.*

Furthermore, assume that $\mathcal{M} = \mathcal{M}_1 \sharp \cdots \sharp \mathcal{M}_\kappa$, and that $\mathcal{H}_k(\widehat{\mathrm{SC}}^{(i)}) \simeq \mathcal{H}_k(\mathcal{M}_i)$ for $i = 1, \cdots, \kappa$.

4

This assumption is the minimal assumption needed for the analysis of the embedding of the $\mathcal{L}_k$; it states that any procedure to construct the simplicial complex or weight function for $\mathcal{L}_k$ is accepted as long as the isomorphic condition holds. The construction of the SC from the point cloud is out of the scope of this manuscript (see, e.g., Chen et al. [12] for building $\mathcal{L}_1$ from $\mathbf{X}$ with an analyzable limit and Latschev's theorem [32] on VR complexes). The last condition requires that the manifold $\mathcal{M}$ can be decomposed; this is most likely true, except for the known hard case of $\mathcal{M}$ with $d = 4$ discussed in Section 2. Note that Assumption 1 is similar to those used in the multi-manifold clustering [54], where they required the manifold to be constructed by a κ-fold union $\mathcal{M} = \mathcal{M}_1 \cup \cdots \cup \mathcal{M}_\kappa$. The goal of our framework is to analyze the homology embedding of k-Laplacian. By contrast, Trillos et al. [54] are interested in identifying each manifold with the notion of clustering ($\mathcal{H}_0$).

Assumption 1 is for points sampled from manifold $\mathcal{M}$ only. To make this assumption hold for networks or images, one can require that the $\mathcal{L}_k$ constructed from these two datasets can be roughly factorized into block-diagonal entries. Below we provide two other assumptions that are valid for both SC and CB (with some modifications): the first one controls the eigengap and the second one ensures a small perturbation in the spectral norm of $\mathcal{L}_k - \widehat{\mathcal{L}}_k$. By construction, $\mathcal{L}_k$ is positive semi-definite; since we are interested in the stability of its null space, we define, for any matrix $\mathbf{L} \succeq 0$, the *eigengap* as the smallest *non-zero* eigenvalue of $\mathbf{L}$ and denote it $\lambda_{\min}(\mathbf{L})$.

Assumption 2. *We denote the set of non-intersecting simplices be $\mathfrak{N}_k := \Sigma_k \cap \widehat{\Sigma}_k$. Let the set of destroyed and created k-simplices during connected sum by $\mathfrak{D}_k$ and $\mathfrak{C}_k$, respectively; they are defined by $\mathfrak{C}_k := \Sigma_k \backslash \mathfrak{N}_k$ and $\mathfrak{D}_k := \widehat{\Sigma}_k \backslash \mathfrak{N}_k$. We have: (1) no k-homology class is created during the connected sum process, i.e., $\beta_k(\text{SC}) = \sum_{i=1}^\kappa \beta_k(\widehat{\text{SC}}^{(i)})$. (2) The eigengaps of $\mathcal{L}_k^{\mathfrak{C},\mathfrak{C}}$ and $\widehat{\mathcal{L}}_k^{\mathfrak{D},\mathfrak{D}}$ are bounded away from the eigengaps of $\mathcal{L}_k^{(ii)}$, i.e., $\min\{\lambda_{\min}(\mathcal{L}_k^{\mathfrak{C},\mathfrak{C}}), \lambda_{\min}(\widehat{\mathcal{L}}_k^{\mathfrak{D},\mathfrak{D}})\} \gg \min\{\delta_1, \cdots, \delta_\kappa\}$, where δ_i is the eigengap of $\mathcal{L}_k^{(ii)}$.*

The first condition requires that the intersecting simplices $\mathfrak{D}_k \cup \mathfrak{C}_k$ do not create or destroy any k-th homology class; this holds, for instance, when the manifold $\mathcal{M}$ has dimension $d > k$. Under this condition, we have $\mathcal{H}_k(\mathcal{M}_1 \sharp \mathcal{M}_2) \simeq \mathcal{H}_k(\mathcal{M}_1) \oplus \mathcal{H}_k(\mathcal{M}_2)$ [33]. A counterexample for this condition is, e.g., inspecting the cavity space ($k = 2$) of a genus-2 surface built from gluing two tori together. That is, β_2 of a genus-2 surface is 1, while the sum of β_2 of two tori is 2. The second condition requires that the principal submatrix of $\mathcal{L}_k$ described by the block of $\mathfrak{C}_k \cup \mathfrak{D}_k$ has large eigengap. This happens, e.g., when $\mathfrak{C}_k$ and $\mathfrak{D}_k$ are cliques and are contained in small balls.

Assumption 3 (Informal). *Let $\tilde{\mathbf{w}}_k = |\mathbf{B}_{k+1}[\mathfrak{N}_k, \mathfrak{N}_{k+1}]|\mathbf{w}_{k+1}$, $\tilde{\mathbf{w}}_{k-1} = |\mathbf{B}_k[:, \mathfrak{N}_k]|\tilde{\mathbf{w}}_k$. For $\ell = k$ or $k - 1$, we have $\max_{\sigma \in \mathfrak{N}_\ell} \{w_\ell(\sigma)/\tilde{w}_\ell(\sigma) - 1\} \leq \epsilon_\ell$, $\max_{\sigma \in \mathfrak{N}_\ell} \{\widehat{w}_\ell(\sigma)/\tilde{w}_\ell(\sigma) - 1\} \leq \epsilon_\ell$, and $\max_{\sigma \in \mathfrak{N}_\ell} \{|w_\ell(\sigma)/\widehat{w}_\ell(\sigma) - 1|\} \leq \epsilon_\ell'$. Assumption S1 is the formal version of this assumption.*

For $k = 1$, it states that not too many triangles are being created or destroyed during connected sum. For this assumption to hold, the sampling density in the connected sum region should be smaller than in other regions, i.e., the manifold $\mathcal{M}$ should be sparsely connected (e.g., Figure 2a). Empirically, we observed that the perturbation is small even when $\mathcal{M}$ is not sparsely connected (more discussions in Section 6). Note also that $\epsilon_\ell' \ll \epsilon_\ell$, for ϵ_ℓ' represents the *net* change in the degree after connected sum. It might be possible to obtain a tighter bound fully by ϵ_ℓ''s, which do not depend on the relative density between the connected sum region and the remaining manifolds; we leave it as future work.

Theorem 1. *Let $\text{DiffL}_k^{\text{down}}$ ($\text{DiffL}_k^{\text{up}}$) be the modified difference (defined in Supplement A) of $\mathcal{L}_k^{\text{down}}$ and $\widehat{\mathcal{L}}_k^{\text{down}}$ (respectively $\mathcal{L}_k^{\text{up}}$ and $\widehat{\mathcal{L}}_k^{\text{up}}$). Under Assumptions 1–3 with notations defined as before and $\lambda_k = k + 2$, if $\left\| \text{DiffL}_k^{\text{down}} \right\|^2 \leq \left[2\sqrt{\epsilon_k'} + \epsilon_k' + \left(1 + \sqrt{\epsilon_k'} \right)^2 \sqrt{\epsilon_{k-1}'} + 4\sqrt{\epsilon_{k-1}} \right]^2 \lambda_{k-1}^2$ and $\|\text{DiffL}_k^{\text{up}}\|^2 \leq \left[2\sqrt{\epsilon_k'} + \epsilon_k' + 2\epsilon_k + 4\sqrt{\epsilon_k} \right]^2 \lambda_k^2$, then there exists a unitary matrix $\mathbf{O} \in \mathbb{R}^{\beta_k \times \beta_k}$ such that*

$$\left\| \mathbf{Y}_{\mathfrak{N}_k,:} - \widehat{\mathbf{Y}}_{\mathfrak{N}_k,:} \mathbf{O} \right\|_F^2 \leq \frac{8\beta_k \left[\left\| \text{DiffL}_k^{\text{down}} \right\|^2 + \|\text{DiffL}_k^{\text{up}}\|^2 \right]}{\min\{\delta_1, \cdots, \delta_\kappa\}}. \tag{2}$$

The proof (in Supplement A) is based on bounding the error between $\mathcal{L}_k$ and $\widehat{\mathcal{L}}_k$ with $\tilde{\mathcal{L}}_k$ (the Laplacian after removal of k-simplices during connected sum), the use of a variant of the Davis-

5

Kahan theorem [61], and the bound of the spectral norm of $\mathcal{L}_k$ for a simplicial complex, i.e., $\|\mathcal{L}_k\|_2 \leq \lambda_k = k + 2$ [26].

The LHS of (2) contains only the simplices in $\mathfrak{N}_k$ because $\mathbf{Y}$ is not defined on $\mathfrak{D}_k$ (similar for $\widehat{\mathbf{Y}}$ and $\mathfrak{C}_k$). Nonetheless, (2) makes sure that the (unbounded) perturbations in the embedding of $\mathfrak{C}_k \cup \mathfrak{D}_k$ do not propagate to the rest of the simplices. The bound in (2) can be extended to CB (Corollary 2) by changing the λ_k value from $(k+2)$ to $2k+2$. The $2k+2$ term here is the maximum eigenvalue of the $\mathcal{L}_k$ built from any cubical complex (Proposition S3).

Corollary 2 (For $\mathcal{L}_k$ built from a CB). *Under Assumptions 2–3 with* $\mathsf{DiffL}_k^{\mathrm{up}}$ *as well as* $\mathsf{DiffL}_k^{\mathrm{down}}$ *defined in Theorem 1 and $\lambda_k = 2k + 2$, there exists a unitary matrix $\mathbf{O}$ such that* (2) *holds.*

Algorithm 1: Subspace identification

Input : SC, k, weights $\mathbf{W}_{k+1}$
1 $\mathbf{B}_k, \mathbf{B}_{k+1} = \mathrm{BOUNDARYMAPS}(\mathrm{SC}, k)$
    ▷ in Algorithm S2
2 **for** $\ell = k, k - 1$ **do**
3      $\mathbf{W}_\ell \leftarrow \mathrm{diag}\{|\mathbf{B}_{\ell+1}|\mathbf{W}_{\ell+1}\mathbf{1}_{n_{\ell+1}}\}$
4      $\mathbf{A}_{\ell+1} \leftarrow \mathbf{W}_\ell^{-1/2}\mathbf{B}_{\ell+1}\mathbf{W}_{\ell+1}^{1/2}$
5 $\mathcal{L}_k = \mathbf{A}_k^\top \mathbf{A}_k + \mathbf{A}_{k+1}\mathbf{A}_{k+1}^\top$
6 $\mathbf{Y} \in \mathbb{R}^{n_k \times \beta_k} \leftarrow \mathrm{NULLSPACE}(\mathcal{L}_k)$
7 $\mathbf{Z} \leftarrow \mathrm{ICANOPREWHITE}(\mathbf{Y})$
Return : Independent basis $\mathbf{Z}$

Subspace $\mathcal{H}_k(\mathcal{M}_i)$ identification. We propose to approximately recover $\widehat{\mathbf{Y}}$ from the columns of the coupled basis $\mathbf{Y}$ by *blind source separation*, as described by Algorithm 1. Specifically, the *independent basis* $\mathbf{Z}$ is obtained by Infomax ICA [6] on $\mathbf{Y}$ of $\mathcal{L}_k$, with a modification (Line 7) that preserves the necessary properties of harmonic cochains (i.e., they are *divergence-free* and *curl-free*, see also Proposition 3). Algorithm 1 works for CB as well by using the appropriate $\mathbf{B}_k$, $\mathbf{B}_{k+1}$ construction method (Line 1). Each column of the obtained $\mathbf{Z}$ is now approximately supported on a single prime manifold $\mathcal{M}_i$.

5 Applications: homologous loops detection, clustering, and visualization

Homologous loop detection. In addition to the *rank* information, one might find it beneficial to extract the shortest cycle of the corresponding $\mathcal{H}_k$ generator. This application is found useful in domains including finding minimum energy trajectories in molecular dynamics datasets, trajectory inference in RNA single-cell sequencing [46], and segmenting circular structures in medical images [50]. We propose a *spectral* shortest homologous loop detection algorithm (Algorithm 2) based on the shortest path algorithm (Dijkstra) as follows: for each dimension $i = 1, \cdots, \beta_1$, the algorithm reverses every edge e having negative $[\mathbf{z}_i]_e$ to generate a weighted digraph $G_i = (V, E_i)$ (Lines 2–4), with the weight of edge $e = (j, j') \in E_i$ equal to the

---

Algorithm 2: Spectral homologous loop detection

Input : $\mathbf{Z} = [\mathbf{z}_1, \cdots, \mathbf{z}_{\beta_1}]$, V, E, edge distance $\mathbf{d}$
1 **for** $i = 1, \cdots, \beta_1$ **do**
2      $E_i^+ \leftarrow \{(s,t) : (s,t) \in E \text{ and } [\mathbf{z}_i]_{(s,t)} > 0\}$
3      $E_i^- \leftarrow \{(t,s) : (s,t) \in E \text{ and } [\mathbf{z}_i]_{(s,t)} < 0\}$
4      $\tau \leftarrow \mathrm{PERCENTILE}(|\mathbf{z}_i|, 1 - 1/\beta_1)$
5      $E_i^\times \leftarrow \{e \in E_i^+ \cup E_i^- : |[\mathbf{z}_i]_e| < \tau\}$
6      $E_i \leftarrow E_i^+ \cup E_i^- \backslash E_i^\times$
7      $G_i \leftarrow (V, E_i)$, with weight of $e \in E_i$ being $[\mathbf{d}]_e$
8      $d_{\min} = \texttt{inf}$
9   **for** $e = (t, s_0) \in E_i$ **do**
10       $\mathcal{P}^*, d^* \leftarrow \mathrm{DIJKSTRA}(G_i, \texttt{from=}s_0, \texttt{to=}t)$
       ▷ Note that $\mathcal{P}^* = [s_0, s_1, \cdots, t]$
11   **if** $d^* < d_{\min}$ **then**
12         $\mathcal{C}_i \leftarrow [t, s_0, s_1, \cdots, t]$
Return : $\mathcal{C}_1, \cdots, \mathcal{C}_{\beta_1}$

Euclidean distance $[\mathbf{d}]_{(j,j')} = \|\mathbf{x}_j - \mathbf{x}_{j'}\|_2$. The algorithm finds a shortest (in terms of $\mathbf{d}$) loop on this weighted digraph for each i and outputs it as the homologous loop representing the i-th class. We present the following proposition (with the proof in Supplement B) to support Algorithm 2; it implies that if each coordinate of $\mathbf{Z}$ extracted from Algorithm 1 corresponds to a homology class, then the detected homologous loop for each homology class is the shortest.

Proposition 3. *Let $\mathbf{z}_i$ for $i = 1, \cdots, \beta_1$ be the i-th homology basis that corresponds to the i-th homology class. For every $i = 1, \cdots, \beta_1$, (1) there exist at least one* cycle *in the digraph G_i such that every vertex $v \in V$ can traverse back to itself (*reachable*); (2) the corresponding* cycle *will enclose at least one homology class (*no short-circuiting*).*

6

Since every vertex is *reachable* from itself, we are guaranteed to find a loop for any starting/ending pair (Lines 9–12). Additionally, there will be no short-circuiting for any loop; each loop we found from Dijkstra is guaranteed to be non-trivial. However, there is one caveat from the second property: even though the i-th loop is non-trivial, it might not always be corresponding to the i-th homology class due to the noise in small $[\mathbf{z}_i]_e$. Namely, loops that do not represent i-th homology class can be formed with edges e having small $[\mathbf{z}_i]_e$, resulting in the instability and the (possible) duplication of the identified loops. To address the issue, we propose a heuristic thresholding, by which we keep the n_1/β_1 edges with the largest absolute value in $|[\mathbf{z}_i]_e|$ (Lines 4–5). We chose to keep n_1/β_1 by treating each homology class equally, i.e., each class has roughly n_1/β_1 edges. Unlike Theorem 1 or Algorithm 1, Algorithm 2 cannot be extended to the case when $k \geq 2$ because the Dijkstra algorithm is employed. We leave its generalization to extract higher-order cavities as future work.

Compared with the previous approach that finds the shortest loops [16] combinatorially, our approach has better time complexity; specifically, the algorithm by Dey et al. [16] has time complexity $\mathcal{O}(nn_1^3 + nn_1^2 n_2)$, whereas Algorithm 2 runs in time $\mathcal{O}(n_1^{2.37\cdots} + \beta_1^2 n_1 + \beta_1 n_1 n \log n)$. The first, second, and third terms correspond to the time complexity of eigendecomposition of $\mathcal{L}_1$, the Info-max ICA, and the Dijkstra algorithm on every digraph G_i, respectively. Note that if the simplicial complex is built from point clouds, the number of triangles n_2 may be large; this dependency on n_2 makes the algorithm [16] hard to scale. On the other hand, our framework requires that $\mathbf{z}_i$ are each supported on one homology class; therefore, loops can only be correctly identified using Algorithm 2 if the manifold is sparsely connected (Assumptions 1–3). Additional comparisons between our algorithm and other methods that pose special requirements on the analyzed data can be found in Supplement D.4.2.

Classifying any 2-dimensional manifold. The Betti number β_1 of a torus is 2, which is equal to that of two disjoint circles; hence one cannot distinguish these two manifolds *only* by rank information. Fortunately, they can be categorized using the homology embedding $\mathbf{Z}$. By the classification theorem [3], any 2D surface is the connected sum of circles $\mathbb{S}^1$ and tori $\mathbb{T}^1$; therefore, Theorem 1 indicates that embedding lies approximately in the directed sum of homology subspace of $\mathbb{S}^1$ and/or $\mathbb{T}^2$. The homology embedding of $\mathbb{S}^1$ is a line since it is in $\mathbb{R}^1$. On the other hand, any loop in a torus can be a convex combination of the two homology classes, implying that the intrinsic dimension of the homology embedding is 2. It is hard to obtain $\mathbf{Z}$ of any arbitrary torus; we present the homology embedding of the flat m-torus below by expressing the null space basis (1-cochains) as the path integrals of the corresponding harmonic 1-forms [12, 59].

Proposition 4. *The envelope of the first homology embedding (1-cochain) induced by the harmonic 1-form on the flat m-torus $\mathbb{T}^m$ is an m-dimensional ellipsoid.*

The proof (in Supplement B) is straightforward thus is omitted here. Proposition 4 and the classification theorem suggest that the first homology embedding is either a line, a disk, or a combination of the two (with replacement). See an example for the genus-2 surface in Figures 2j and S1.

Note that it is possible to classify any 2-manifold with higher-dimensional homology groups; for instance, one can distinguish $\mathbb{T}^2$ from $\mathbb{S}^1 \sharp \mathbb{S}^1$ by the second homology group. However, our approach scales better in computation or memory usage since inspecting $\mathcal{H}_2$ needs at least the calculation and storage of tetrahedrons from the neighborhood graph.

Other applications. As pointed out earlier, one can visualize the basis of the harmonic vector fields (of $\mathcal{H}_k$) by overlaying the columns of $\mathbf{Y}$ onto the original dataset (Figure 1). Being able to successfully extract a decoupled basis $\mathbf{Z}$ increases the interpretability of $\mathcal{H}_k$, as shown in the second row of Figure 1. Theorem 1 also supports the use of subspace clustering algorithm in the higher-order simplex clustering framework [21].

6 Experiments

We demonstrate our approach by computing $\mathbf{Y}, \mathbf{Z}$ and the shortest loops for five synthetic manifolds: two of them are prime manifolds (TORUS *torus*, 3-TORUS *three-torus*) and three (PUNCTPLANE *punctured plane with two holes*, GENUS-2 *genus-2*, and TORI-CONCAT *concatenation of 4 tori*) are factorizable manifolds. Furthermore, five additional real point clouds (ETH and MDA from chemistry, PANCREAS from biology, 3D-GRAPH from 3D modeling, and ISLAND from oceanography) are ana-

7
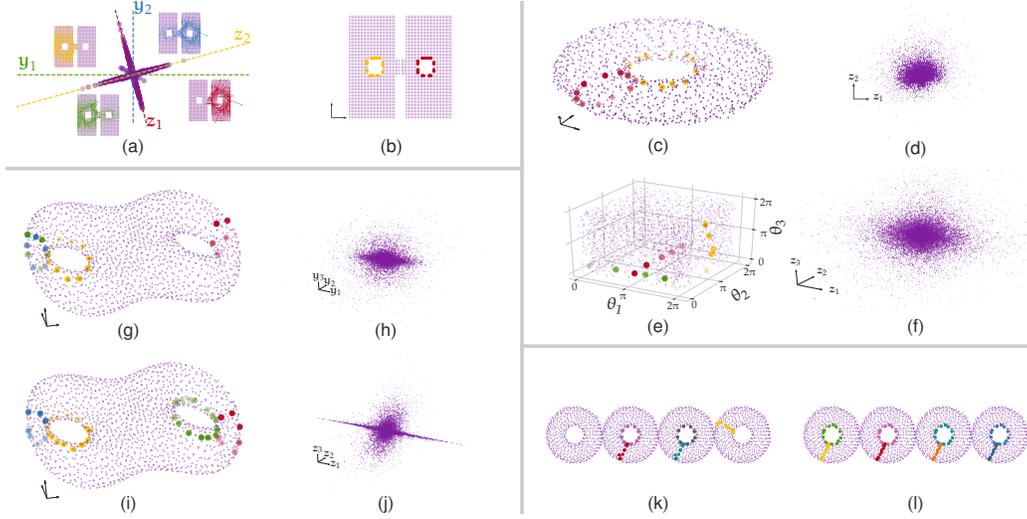
Figure 2: (a) The first homology embedding of PUNCTPLANE. The harmonic vector fields are overlaid on the data in the inset plots; green, blue, red, and yellow arrows correspond to $\mathbf{y}_1$, $\mathbf{y}_2$, $\mathbf{z}_1$, and $\mathbf{z}_2$, respectively. (b), (c), (e), (i), and (l) are the detected loops using Dijkstra on $\mathbf{Z}$ for PUNCTPLANE (colors are in (a)), TORUS, 3-TORUS, GENUS-2, and TORI-CONCAT, respectively. (g) and (k) represent the identified loops on the coupled embedding $\mathbf{Y}$ for GENUS-2 and TORI-CONCAT, respectively. (d), (f), (h), and (j) present the embeddings used to detect loops in (c), (e), (g), and (i), respectively.

lyzed under this framework. For all the point clouds, we build the VR complex SC from the CkNN kernel [8] so that the resulting $\mathcal{L}_1$ is sparse and the topological information is preserved. Note that other methods for building an SC from $\mathbf{X}$ can also be used as long as $\mathcal{H}_k$ is successfully identified (Assumption 1). Lastly, we illustrate the efficacy of our framework to a non-manifold data: RETINA from medical imaging. Please refer to Supplement D for detailed discussions on procedures to generate, preprocess, and download these datasets. All experiments are replicated more than five times with similar results. We perform our analysis on a desktop running Linux with 32GB RAM and an 8-Core 4.20GHz Intel® Core™ i7-7700K CPU; every experiment completes within 3 minutes (1-2 minutes on eigendecomposition of $\mathcal{L}_1$, and around 30 seconds on both ICA and Algorithm 2).

Synthetic manifolds. The results for the synthetic manifolds are in Figure 2. Figure 2a (the harmonic embedding of PUNCTPLANE) confirms Theorem 1 that $\mathbf{Y}$ is approximately distributed on two subspaces (yellow and red), with each loop parametrizing a single hole (inset of Figure 2a). As discussed previously in Figure 1, the harmonic vector bases (green and blue) are mixtures of the separate subspaces; therefore, these bases have poor interpretability compared with the independent subspace $\mathbf{Z}$ identified by Algorithm 1. The shortest loops (Figure 2b) corresponding to $\mathbf{z}_1$ (yellow), $\mathbf{z}_2$ (red) are obtained by running Dijkstra on the digraphs induced by $\mathbf{z}_1$ and $\mathbf{z}_2$ separately (Algorithm 2). Figures 2c–2f show the results of the two simple *prime manifolds*: TORUS and 3-TORUS. The harmonic embeddings of TORUS (Figure 2d) and 3-TORUS (Figure 2f) are a two-dimensional disk and a three-dimensional ellipsoid, respectively; this confirms the conclusion from Proposition 4. The shortest loops obtained from Algorithm 2 for these two datasets are in Figures 2c and 2e, showing that these loops travel around the holes in TORUS (or 3-TORUS). Note that we plot 3-TORUS in the intrinsic coordinate because a three torus can not be embedded in 3D without breaking neighborhood relationships. Three lines in 2e are indeed loops due to the periodic boundary condition, i.e., $0 = 2\pi$, in the intrinsic coordinate. Figures 2h and 2j show the embedding of the coupled harmonic basis ($\mathbf{Y}$) and that corresponding to the independent subspace ($\mathbf{Z}$) obtained by Algorithm 1. Compared with $\mathbf{Y}$, each coordinate of $\mathbf{Z}$ corresponds to a subspace, i.e., the left or right handle of GENUS-2, and does not couple with other homology generators. $\mathbf{Z}$ is thus a union of two 2D disks, with each disk approximating the harmonic embedding of a torus (see Figure S1 for more detail). Compared with the loops obtained by running Algorithm 2 on $\mathbf{Y}$ (Figure 2g), each loop in Figure 2i identified from $\mathbf{Z}$ parameterizes the corresponding homology generator without being homologous to other loops. Similar results on TORI-CONCAT are in Figures 2k and 2l, which correspond to the

8
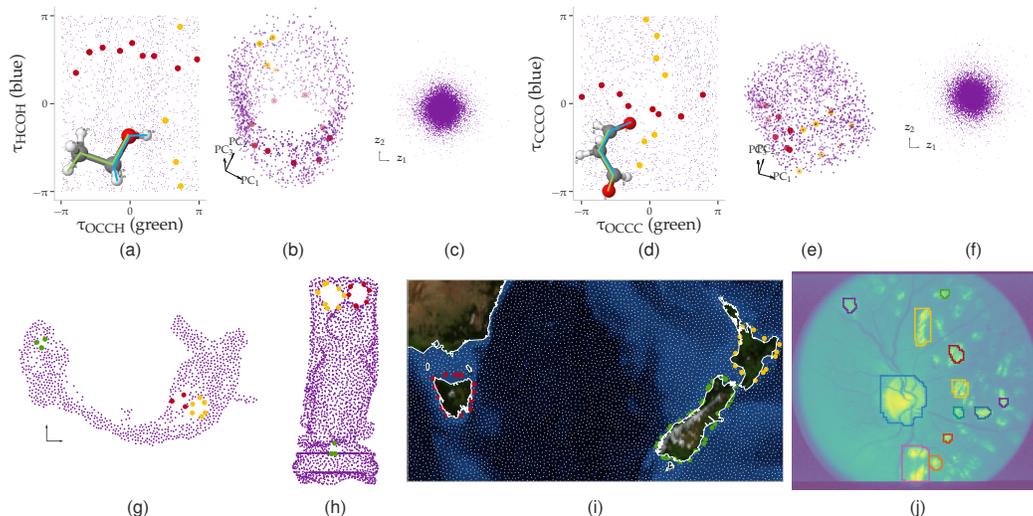
Figure 3: (a) and (b) are the detected loops of ETH using Dijkstra on $\mathbf{Z}$ (in (c)) in the torsion space (inset of (a)) and in the PCA space, respectively. (d)–(f) are the results for MDA that are similar to those for ETH in (a)–(c). (g)–(j) show the identified loops using $\mathbf{Z}$ for PANCREAS, 3D-GRAPH, ISLAND, and RETINA, respectively.

loops obtained from $\mathbf{Y}$ and $\mathbf{Z}$, respectively. The pairwise scatter plots of the eight-dimensional $\mathbf{Z}$ (or $\mathbf{Y}$) are in Figure S2 of Supplement D. Note that PUNCTPLANE is an example of a sparsely connected manifold (see the low-density area in the middle), with $\epsilon_1 \approx 0.035$ and $\epsilon_0 \approx 0.038$. Manifolds of other synthetic/real datasets might not be sparsely connected due to the (approximately) constant sampling densities; nevertheless, the perturbations to the subspaces remain small for these datasets.

Small molecule data [13]. Figures 3a–3c and 3d–3f show our analysis on ETH and MDA, respectively. These two small molecule datasets, whose ambient dimensions are $D = 102$ and $D = 98$, are suggested to be noisy non-uniformly sampled tori [52]; the harmonic embeddings of these two datasets (Figures 3c and 3f) confirm this idea. Finding the minimum trajectories corresponding to a specific bond torsion is of interest in chemistry; in these two molecular dynamics systems, this problem can be translated into finding the homologous loops in the point cloud. The homologous loops found by Algorithm 2 overlaid on the first three *principal components* (PCs) for these two datasets can be found in Figures 3b (for ETH) and 3e (for MDA). The same homologous loops plotted in the bond torsion space (with definition in the insets) based on our prior knowledge are in Figures 3a and 3d. Similar to the discussion for 3-TORUS (Figure 2e), the yellow/red trajectories form loops due to the periodic boundary condition of the bond torsions.

RNA single-cell sequencing data [7]. The *trajectory inference* methods [46] for analyzing the RNA single-cell sequencing datasets aim to order the cells (points in high-dimensional expression space) along developmental trajectories, which are inferred from the structure of the point clouds. Identifying loops in the dataset can serve as a building block for delineating a correct trajectory, especially for determining cell cycle and cell differentiation. To illustrate the idea, we compute the 1-Laplacian on the CkNN kernel [8] constructed on the UMAP [36] embedding (Algorithm 1). Figure 3g shows the identified loops from Algorithm 2, with the green loop being the cycle of ductal cells and yellow/red loops representing a trifurcation (endocrine cell differentiation).

Additional point cloud datasets. 3D-GRAPH [15] is a 3D model of a Buddha statue with a pre-computed triangulation. We treat the 3D model as a point cloud and subsample 3000 farthest points from the original dataset; $\mathcal{L}_1$ is obtained from the VR complex of the CkNN kernel. Note that with this small sample size, two smaller loops near the waist of the statue are not detectable. Hence, the number of zero eigenvalues of $\mathcal{L}_1$ is 3, with the corresponding homology generators shown in Figure 3h. ISLAND [23], which contains ocean buoys around the Tasman sea, is the other point cloud in

9

our analysis. The estimated β_1 is 3, with the detected loops being the North Island of New Zealand, the South Island of New Zealand, and the main island of Tasmania (Figure 3i).

Non-manifold dataset. Our framework for identifying subspaces is still valid for cubical complexes built from images (by Corollary 2). We demonstrate the idea on RETINA, a medical retinal image [25]. The cubical complex is constructed by intensity thresholding (also called the sub-level set method in TDA [58]) and then applying morphological closing on the binary image to remove small cavities. The weight for every rectangle $\mathbf{w}_2(\sigma)$ is set to 1; the estimated null space dimension of the $\mathcal{L}_1$ built from CB is $\beta_1 = 12$, with the identified homologous loops in Figure 3j. The result shows the robustness of the proposed framework even for large β_1.

7 Conclusion and broader impact

Our contributions in the emerging field of spectral algorithms for k-Laplacians $\mathcal{L}_k$ [12, 21, 35, 48] are summarized as follows. (i) We extend the study of the homology embedding of vertices by the graph Laplacian $\mathcal{L}_0$ (spectral clustering) to those of higher-order simplices by $\mathcal{L}_k$. Specifically, the k-th homology embedding can be approximately factorized into parts, with each corresponding to a prime manifold given a small perturbation (small ϵ_ℓ and ϵ'_ℓ for $\ell = k, k-1$). (ii) The analysis is made possible by expressing the κ-fold *connected sum* as a matrix perturbation. This convenient property of the homology embedding supports (iii) the use of ICA to identify each decoupled subspace and motivates (iv) the application to the shortest homologous loop detection problem. The proposed framework opens up numerous future directions for us to explore. For instance, one can extend our framework to investigate the generalization of the loosely connected clusters, i.e., when the null space $\mathcal{H}_k$ eigenvalues are not strictly zero; it applies to the case when analyzing the noisy topological structures in the data manifold. Moreover, the connections of our framework to the recent advances in spectral TDA and representation learning can be further explored; they include the persistent spectral method [38, 57] and the disentanglement of representation [63] in generative modeling.

Broader impact. Our analysis provides insight into the structure of the k-th harmonic embedding. This framework can inspire researchers in developing *spectral* topological data analysis algorithms (e.g., visualization, clustering, tightest higher-order *cycles* for $k \geq 2$ [20, 42]) similar to those that were inaugurated by spectral clustering two decades ago. These applications are especially beneficial to scientists (chemists, biologists, oceanographers, etc.) who use high-dimensional data analysis techniques for studying complex systems. Similar to the limitation of other unsupervised learning algorithms, practitioners without solid understandings of *both* the analyzed datasets and the used algorithm might draw controversial conclusions (see, e.g., discussions in [2, 41]). Possible approaches to mitigate the negative consequences are to design proper validation and causal inference algorithms for this framework; we leave them as potential directions we will explore.

Acknowledgements

The authors acknowledge partial support from the U.S. Department of Energy's Office of Energy Efficiency and Renewable Energy (EERE) under the Solar Energy Technologies Office Award Number DE-EE0008563 and from the National Science Foundation award DMS 2015272. They thank Alexandre Tkatchenko, Jim Pfaendtner, Stefan Chmiela, and Chris Fu for providing the molecular dynamics data as well as for many hours of brainstorming and advice.

Disclaimer

The views expressed herein do not necessarily represent the views of the U.S. Department of Energy or the United States Government.

References

[1] Saad Ali, Arslan Basharat, and Mubarak Shah. Chaotic Invariants for Human Action Recognition. In *2007 IEEE 11th International Conference on Computer Vision*, pages 1–8, October 2007. doi: 10.1109/ICCV.2007.4409046.

10

[2] Jose Alquicira-Hernandez, Joseph Powell, and Tri Giang Phan. No evidence that plasmablasts transdifferentiate into developing neutrophils in severe COVID-19 disease. *bioRxiv*, 2020.

[3] Mark Anthony Armstrong. *Basic Topology*. Springer Science & Business Media, 2013.

[4] Sergio Barbarossa and Stefania Sardellitti. Topological signal processing over simplicial complexes. *IEEE Transactions on Signal Processing*, 68:2992–3007, 2020.

[5] Mikhail Belkin and Partha Niyogi. Laplacian Eigenmaps for Dimensionality Reduction and Data Representation. *Neural Computation*, 15(6):1373–1396, June 2003. ISSN 0899-7667. doi: 10.1162/089976603321780317.

[6] Anthony J. Bell and Terrence J. Sejnowski. An information-maximization approach to blind separation and blind deconvolution. *Neural computation*, 7(6):1129–1159, 1995.

[7] Volker Bergen, Marius Lange, Stefan Peidli, F. Alexander Wolf, and Fabian J. Theis. Generalizing RNA velocity to transient cell states through dynamical modeling. *Nature biotechnology*, 38(12):1408–1414, 2020.

[8] Tyrus Berry and Timothy Sauer. Consistent manifold representation for topological data analysis. *Foundations of Data Science*, 1(1):1, 2019. doi: 10.3934/fods.2019001.

[9] Imre Bokor, Diarmuid Crowley, Stefan Friedl, Fabian Hebestreit, Daniel Kasprowski, Markus Land, and Johnny Nicholson. Connected sum decompositions of high-dimensional manifolds. *arXiv:1909.02628 [math]*, September 2020.

[10] Oleksiy Busaryev, Sergio Cabello, Chao Chen, Tamal K. Dey, and Yusu Wang. Annotating simplices with a homology basis and its applications. In *Scandinavian Workshop on Algorithm Theory*, pages 189–200. Springer, 2012.

[11] Erin W. Chambers, Jeff Erickson, and Amir Nayyeri. Minimum cuts and shortest homologous cycles. In *Proceedings of the Twenty-Fifth Annual Symposium on Computational Geometry*, pages 377–385, 2009.

[12] Yu-Chia Chen, Marina Meilă, and Ioannis G. Kevrekidis. Helmholtzian Eigenmap: Topological feature discovery & edge flow learning from point cloud data. *arXiv:2103.07626 [stat.ML]*, March 2021.

[13] Stefan Chmiela, Alexandre Tkatchenko, Huziel E Sauceda, Igor Poltavsky, Kristof T Schütt, and Klaus-Robert Müller. Machine learning of accurate energy-conserving molecular force fields. *Science advances*, 3(5):e1603015, 2017.

[14] Ronald R. Coifman and Stéphane Lafon. Diffusion maps. *Applied and Computational Harmonic Analysis*, 21(1):5–30, July 2006. ISSN 1063-5203. doi: 10.1016/j.acha.2006.04.006.

[15] Brian Curless and Marc Levoy. A volumetric method for building complex models from range images. In *Proceedings of the 23rd Annual Conference on Computer Graphics and Interactive Techniques*, pages 303–312, 1996.

[16] Tamal K. Dey, Jian Sun, and Yusu Wang. Approximating loops in a shortest homology basis from point data. In *Proceedings of the Twenty-Sixth Annual Symposium on Computational Geometry*, pages 166–175, 2010.

[17] Tamal K. Dey, Anil N. Hirani, and Bala Krishnamoorthy. Optimal Homologous Cycles, Total Unimodularity, and Linear Programming. *SIAM Journal on Computing*, 40(4):1026–1044, January 2011. ISSN 0097-5397. doi: 10.1137/100800245.

[18] Tamal K. Dey, Fengtao Fan, and Yusu Wang. An efficient computation of handle and tunnel loops via Reeb graphs. *ACM Transactions on Graphics (TOG)*, 32(4):1–10, 2013.

[19] Tamal K. Dey, Tao Hou, and Sayan Mandal. Persistent 1-cycles: Definition, computation, and its application. In *International Workshop on Computational Topology in Image Context*, pages 123–136. Springer, 2019.

11

[20] Tamal K. Dey, Tao Hou, and Sayan Mandal. Computing minimal persistent cycles: Polynomial and hard cases. In *Proceedings of the Fourteenth Annual ACM-SIAM Symposium on Discrete Algorithms*, pages 2587–2606. SIAM, 2020.

[21] Stefania Ebli and Gard Spreemann. A Notion of Harmonic Clustering in Simplicial Complexes. *2019 18th IEEE International Conference On Machine Learning And Applications (ICMLA)*, pages 1083–1090, December 2019. doi: 10.1109/ICMLA.2019.00182.

[22] Xin Feng and Yiying Tong. Choking loops on surfaces. *IEEE transactions on visualization and computer graphics*, 19(8):1298–1306, 2013.

[23] Gary Froyland and Kathrin Padberg-Gehle. A rough-and-ready cluster-based approach for extracting finite-time coherent sets from sparse and incomplete trajectory data. *Chaos: An Interdisciplinary Journal of Nonlinear Science*, 25(8):087406, July 2015. ISSN 1054-1500. doi: 10.1063/1.4926372.

[24] Felix Hensel, Michael Moor, and Bastian Rieck. A Survey of Topological Machine Learning Methods. *Frontiers in Artificial Intelligence*, 4:52, 2021.

[25] Adam Hoover and Michael Goldbaum. Locating the optic nerve in a retinal image using the fuzzy convergence of the blood vessels. *IEEE transactions on medical imaging*, 22(8):951–958, 2003.

[26] Danijela Horak and Jürgen Jost. Spectra of combinatorial Laplace operators on simplicial complexes. *Advances in Mathematics*, 244:303–336, September 2013. ISSN 0001-8708. doi: 10.1016/j.aim.2013.05.007.

[27] Junteng Jia, Michael T. Schaub, Santiago Segarra, and Austin R. Benson. Graph-based Semi-Supervised & Active Learning for Edge Flows. In *KDD*, 2019. doi: 10.1145/3292500.3330872.

[28] Xiaoye Jiang, Lek-Heng Lim, Yuan Yao, and Yinyu Ye. Statistical ranking and combinatorial Hodge theory. *Mathematical Programming*, 127(1):203–244, March 2011. ISSN 1436-4646. doi: 10.1007/s10107-010-0419-x.

[29] Dominique Joncas, Marina Meila, and James McQueen. Improved Graph Laplacian via Geometric Self-Consistency. In I. Guyon, U. V. Luxburg, S. Bengio, H. Wallach, R. Fergus, S. Vishwanathan, and R. Garnett, editors, *Advances in Neural Information Processing Systems 30*, pages 4457–4466. Curran Associates, Inc., 2017.

[30] Karin Kailing, Hans-Peter Kriegel, and Peer Kröger. Density-connected subspace clustering for high-dimensional data. In *Proceedings of the 2004 SIAM International Conference on Data Mining*, pages 246–256. SIAM, 2004.

[31] Violeta Kovacev-Nikolic, Peter Bubenik, Dragan Nikolić, and Giseon Heo. Using persistent homology and dynamical distances to analyze protein binding. *Statistical applications in genetics and molecular biology*, 15(1):19–38, 2016.

[32] Janko Latschev. Vietoris-Rips complexes of metric spaces near a closed Riemannian manifold. *Archiv der Mathematik*, 77(6):522–528, 2001.

[33] John M. Lee. Introduction to Smooth Manifolds. In *Introduction to Smooth Manifolds*, pages 1–31. Springer, 2013.

[34] Yin Tat Lee and Aaron Sidford. Path finding methods for linear programming: Solving linear programs in o (vrank) iterations and faster algorithms for maximum flow. In *2014 IEEE 55th Annual Symposium on Foundations of Computer Science*, pages 424–433. IEEE, 2014.

[35] Lek-Heng Lim. Hodge laplacians on graphs. *Siam Review*, 62(3):685–715, 2020.

[36] Leland McInnes, John Healy, and James Melville. Umap: Uniform manifold approximation and projection for dimension reduction. *arXiv preprint arXiv:1802.03426*, 2018.

[37] Marina Meilă and Jianbo Shi. A random walks view of spectral segmentation. In *International Workshop on Artificial Intelligence and Statistics*, pages 203–208. PMLR, 2001.

12

[38] Zhenyu Meng and Kelin Xia. Persistent spectral–based machine learning (PerSpect ML) for protein-ligand binding affinity prediction. *Science Advances*, 7(19):eabc5329, 2021.

[39] John Milnor. A unique decomposition theorem for 3-manifolds. *American Journal of Mathematics*, 84(1):1–7, 1962.

[40] Andrew Y. Ng, Michael I. Jordan, and Yair Weiss. On spectral clustering: Analysis and an algorithm. *Advances in neural information processing systems*, 2:849–856, 2002.

[41] John Novembre and Matthew Stephens. Interpreting principal component analyses of spatial population genetic variation. *Nature genetics*, 40(5):646–649, May 2008. ISSN 1061-4036. doi: 10.1038/ng.139.

[42] Ippei Obayashi. Volume Optimal Cycle: Tightest representative cycle of a generator on persistent homology. *arXiv:1712.05103 [cs, math]*, December 2017.

[43] Nina Otter, Mason A. Porter, Ulrike Tillmann, Peter Grindrod, and Heather A. Harrington. A roadmap for the computation of persistent homology. *EPJ Data Science*, 6(1):17, December 2017. ISSN 2193-1127. doi: 10.1140/epjds/s13688-017-0109-5.

[44] T. Mitchell Roddenberry and Santiago Segarra. HodgeNet: Graph Neural Networks for Edge Data. In *2019 53rd Asilomar Conference on Signals, Systems, and Computers*, pages 220–224. IEEE, 2019.

[45] T. Mitchell Roddenberry, Nicholas Glaze, and Santiago Segarra. Principled simplicial neural networks for trajectory prediction. In *International Conference on Machine Learning*, pages 9020–9029. PMLR, 2021.

[46] Wouter Saelens, Robrecht Cannoodt, Helena Todorov, and Yvan Saeys. A comparison of single-cell trajectory inference methods. *Nature biotechnology*, 37(5):547–554, 2019.

[47] Manish Saggar, Olaf Sporns, Javier Gonzalez-Castillo, Peter A. Bandettini, Gunnar Carlsson, Gary Glover, and Allan L. Reiss. Towards a new approach to reveal dynamical organization of the brain using topological data analysis. *Nature communications*, 9(1):1–14, 2018.

[48] Michael T. Schaub, Austin R. Benson, Paul Horn, Gabor Lippner, and Ali Jadbabaie. Random walks on simplicial complexes and the normalized Hodge 1-Laplacian. *SIAM Review*, 62(2): 353–391, 2020.

[49] Geoffrey Schiebinger, Martin J. Wainwright, and Bin Yu. The geometry of kernelized spectral clustering. *Annals of Statistics*, 43(2):819–846, April 2015. ISSN 0090-5364, 2168-8966. doi: 10.1214/14-AOS1283.

[50] Nikhil Singh, Heather D. Couture, J. S. Marron, Charles Perou, and Marc Niethammer. Topological descriptors of histology images. In *International Workshop on Machine Learning in Medical Imaging*, pages 231–239. Springer, 2014.

[51] G. W. Stewart, J. W. Stewart, and Ji-guang Sun. *Matrix Perturbation Theory*. Elsevier Science, July 1990. ISBN 978-0-12-670230-9.

[52] Michael Tabor. *Chaos and Integrability in Nonlinear Dynamics: An Introduction*. Wiley, 1989.

[53] Daniel Ting, Ling Huang, and Michael Jordan. An Analysis of the Convergence of Graph Laplacians. In *Proceedings of the 27th International Conference on Machine Learning (ICML)*, 2010.

[54] Nicolas Garcia Trillos, Pengfei He, and Chenghui Li. Large sample spectral analysis of graph-based multi-manifold clustering. *arXiv preprint arXiv:2107.13610*, 2021.

[55] Ulrike von Luxburg. A Tutorial on Spectral Clustering. *arXiv:0711.0189 [cs]*, November 2007.

[56] Yali Wan and Marina Meila. A class of network models recoverable by spectral clustering. In *NIPS*, pages 3285–3293, 2015.

13

[57] Rui Wang, Duc Duy Nguyen, and Guo-Wei Wei. Persistent spectral graph. *International journal for numerical methods in biomedical engineering*, 36(9):e3376, 2020.

[58] Larry Wasserman. Topological data analysis. *Annual Review of Statistics and Its Application*, 5:501–532, 2018.

[59] Hassler Whitney. *Geometric Integration Theory*. Dover Publications, Mineola, N.Y, December 2005. ISBN 978-0-486-44583-0.

[60] Pengxiang Wu, Chao Chen, Yusu Wang, Shaoting Zhang, Changhe Yuan, Zhen Qian, Dimitris Metaxas, and Leon Axel. Optimal topological cycles and their application in cardiac trabeculae restoration. In *International Conference on Information Processing in Medical Imaging*, pages 80–92. Springer, 2017.

[61] Yi Yu, Tengyao Wang, and Richard J. Samworth. A useful variant of the Davis–Kahan theorem for statisticians. *Biometrika*, 102(2):315–323, 2015.

[62] Rundong Zhao, Menglun Wang, Jiahui Chen, Yiying Tong, and Guo-Wei Wei. The de Rham–Hodge Analysis and Modeling of Biomolecules. *Bulletin of mathematical biology*, 82 (8):1–38, 2020.

[63] Sharon Zhou, Eric Zelikman, Fred Lu, Andrew Y. Ng, Gunnar Carlsson, and Stefano Ermon. Evaluating the disentanglement of deep generative models through manifold topology. *arXiv preprint arXiv:2006.03680*, 2020.

[64] Xiaojin Zhu. Persistent Homology: An Introduction and a New Text Representation for Natural Language Processing. In *Twenty-Third International Joint Conference on Artificial Intelligence*, June 2013.

Checklist

1. For all authors...

   (a) Do the main claims made in the abstract and introduction accurately reflect the paper's contributions and scope? [Yes]

   (b) Did you describe the limitations of your work? [Yes] See Section 4

   (c) Did you discuss any potential negative societal impacts of your work? [Yes] See Section 7

   (d) Have you read the ethics review guidelines and ensured that your paper conforms to them? [Yes]

2. If you are including theoretical results...

   (a) Did you state the full set of assumptions of all theoretical results? [Yes]

   (b) Did you include complete proofs of all theoretical results? [Yes] In Supplement A–C

3. If you ran experiments...

   (a) Did you include the code, data, and instructions needed to reproduce the main experimental results (either in the supplemental material or as a URL)? [Yes] In Supplement D

   (b) Did you specify all the training details (e.g., data splits, hyperparameters, how they were chosen)? [Yes] In Supplement D

   (c) Did you report error bars (e.g., with respect to the random seed after running experiments multiple times)? [N/A] Do not have error bars to report; all experiments are ran at least five times, and we observe similar results.

   (d) Did you include the total amount of compute and the type of resources used (e.g., type of GPUs, internal cluster, or cloud provider)? [Yes] See Section 6

4. If you are using existing assets (e.g., code, data, models) or curating/releasing new assets...

   (a) If your work uses existing assets, did you cite the creators? [Yes] In Supplement D

   (b) Did you mention the license of the assets? [Yes] In Supplement D

14

(c) Did you include any new assets either in the supplemental material or as a URL? [Yes] New codes are attached in the supplemental material `codes.zip`; they can also be found at `https://github.com/yuchaz/homology_emb`. We do not create new datasets.

(d) Did you discuss whether and how consent was obtained from people whose data you're using/curating? [Yes] In Supplement D

(e) Did you discuss whether the data you are using/curating contains personally identifiable information or offensive content? [N/A] Datasets do not contain personal identifiable information.

5. If you used crowdsourcing or conducted research with human subjects...

(a) Did you include the full text of instructions given to participants and screenshots, if applicable? [N/A] No crowdsourcing data nor conducted research with human subjects

(b) Did you describe any potential participant risks, with links to Institutional Review Board (IRB) approvals, if applicable? [N/A] No crowdsourcing data nor conducted research with human subjects

(c) Did you include the estimated hourly wage paid to participants and the total amount spent on participant compensation? [N/A] No crowdsourcing data nor conducted research with human subjects

15

Supplementary Material of
The decomposition of the higher-order homology embedding constructed from the k-Laplacian

Table of Contents

A Proof of subspace perturbations (Theorem 1)   **1**

   A.1   A formal version of Assumption 3   1

   A.2   Definitions of $\mathcal{L}_k$ and $\widehat{\mathcal{L}}_k$ 2

   A.3   Useful lemmas   4

   A.4   Proof of Theorem 1   5

B Proofs of propositions in Applications (Section 5)   **8**

   B.1   Proof of Proposition 3: the properties of the induced digraph   8

   B.2   Proof of Proposition 4: $\mathcal{H}_1$ embedding of $\mathbb{T}^m$ 8

C The maximum eigenvalue of $\mathcal{L}_k$ constructed from a cubical complex   **8**

D Datasets, experiment details, and discussions   **9**

   D.1   Synthetic manifolds   10

   D.2   Real datasets   10

   D.3   Pairwise scatter plots   11

   D.4   Experiments and discussions on the shortest homologous loops detection algorithm   18

E Pseudocodes   **19**

i

A Proof of subspace perturbations (Theorem 1)

A.1 A formal version of Assumption 3

Assumption S1. *Let* $\tilde{\mathbf{w}}_k = |\mathbf{B}_{k+1}[\mathfrak{N}_k, \mathfrak{N}_{k+1}]|\mathbf{w}_{k+1}$, $\tilde{\mathbf{w}}_{k-1} = |\mathbf{B}_k[:, \mathfrak{N}_k]|\tilde{\mathbf{w}}_k$, *with* $\mathbf{w}_k$ *and* $\widehat{\mathbf{w}}_k$ *defined in Section 3. Additionally, write*

$$\mathbf{W}_{k+1} = \tilde{\mathbf{W}}_{k+1} + \boldsymbol{\mathcal{E}}_{k+1,+},$$

$$\widehat{\mathbf{W}}_{k+1} = \tilde{\mathbf{W}}_{k+1} + \boldsymbol{\mathcal{E}}_{k+1,-},$$

$$\mathbf{W}_k^{1/2} = \tilde{\mathbf{W}}_k^{1/2}(\mathbf{I} + \mathbf{E}_{k,+}^+) + \boldsymbol{\mathcal{E}}_{k,+}^{1/2},$$

$$\mathbf{W}_k^{-1/2} = \tilde{\mathbf{W}}_k^{-1/2}(\mathbf{I} - \mathbf{E}_{k,+}^-) + \boldsymbol{\mathcal{E}}_{k,+}^{-1/2},$$

$$\widehat{\mathbf{W}}_k^{1/2} = \tilde{\mathbf{W}}_k^{1/2}(\mathbf{I} + \mathbf{E}_{k,-}^+) + \boldsymbol{\mathcal{E}}_{k,-}^{1/2},$$

$$\widehat{\mathbf{W}}_k^{-1/2} = \tilde{\mathbf{W}}_k^{-1/2}(\mathbf{I} - \mathbf{E}_{k,-}^-) + \boldsymbol{\mathcal{E}}_{k,-}^{-1/2},$$

$$\mathbf{W}_{k-1}^{-1/2} = \tilde{\mathbf{W}}_{k-1}^{-1/2}(\mathbf{I} - \mathbf{E}_{k-1,+}),$$

$$\widehat{\mathbf{W}}_{k-1}^{-1/2} = \tilde{\mathbf{W}}_{k-1}^{-1/2}(\mathbf{I} - \mathbf{E}_{k-1,-}).$$

There exists $\epsilon_\ell > 0$ *and* $\epsilon'_\ell > 0$ *for* $\ell = k, k-1$ *such that the following conditions hold*

1. *Not too many* $(k+1)$*-simplices are created (small* $|\mathfrak{C}_{k+1}|$*)*

$$\|\mathbf{E}_{k,+}^+\| = \max_{\sigma \in \mathfrak{N}_k}\left\{\left[\mathbf{E}_{k,+}^+\right]_{\sigma,\sigma}\right\} = \max_{\sigma \in \mathfrak{N}_k}\left\{\frac{w_k^{1/2}(\sigma)}{\tilde{w}_k^{1/2}(\sigma)} - 1\right\} \leq \sqrt{\epsilon_k}; \qquad \text{(S1a)}$$

$$\|\mathbf{E}_{k,+}^-\| = \max_{\sigma \in \mathfrak{N}_k}\left\{\left[\mathbf{E}_{k,+}^-\right]_{\sigma,\sigma}\right\} = \max_{\sigma \in \mathfrak{N}_k}\left\{\frac{\tilde{w}_k^{-1/2}(\sigma)}{w_k^{-1/2}(\sigma)} - 1\right\} \leq \sqrt{\epsilon_k}; \qquad \text{(S1b)}$$

$$\max_{\sigma \in \mathfrak{N}_k}\left\{\frac{w_k(\sigma)}{\tilde{w}_k(\sigma)} - 1\right\} \leq \epsilon_k; \qquad \text{(S1c)}$$

$$\|\mathbf{E}_{k-1,+}\| = \max_{\nu \in \Sigma_{k-1}}\left\{\left[\mathbf{E}_{k-1,+}\right]_{\nu,\nu}\right\} = \max_{\nu \in \Sigma_{k-1}}\left\{\frac{\tilde{w}_{k-1}^{-1}(\nu)}{w_{k-1}^{-1}(\nu)} - 1\right\} \leq \sqrt{\epsilon_{k-1}}; \qquad \text{(S1d)}$$

$$\max_{\nu \in \Sigma_{k-1}}\left\{\frac{w_{k-1}(\nu)}{\tilde{w}_{k-1}(\nu)} - 1\right\} \leq \epsilon_{k-1}. \qquad \text{(S1e)}$$

2. *Not too many* $(k+1)$*-simplices are destroyed (small* $|\mathfrak{D}_{k+1}|$*)*

$$\|\mathbf{E}_{k,-}^+\| = \max_{\sigma \in \mathfrak{N}_k}\left\{\left[\mathbf{E}_{k,-}^+\right]_{\sigma,\sigma}\right\} = \max_{\sigma \in \mathfrak{N}_k}\left\{\frac{\widehat{w}_k^{1/2}(\sigma)}{\tilde{w}_k^{1/2}(\sigma)} - 1\right\} \leq \sqrt{\epsilon_k}; \qquad \text{(S2a)}$$

$$\|\mathbf{E}_{k,-}^-\| = \max_{\sigma \in \mathfrak{N}_k}\left\{\left[\mathbf{E}_{k,-}^-\right]_{\sigma,\sigma}\right\} = \max_{\sigma \in \mathfrak{N}_k}\left\{\frac{\tilde{w}_k^{-1/2}(\sigma)}{\widehat{w}_k^{-1/2}(\sigma)} - 1\right\} \leq \sqrt{\epsilon_k}; \qquad \text{(S2b)}$$

$$\max_{\sigma \in \mathfrak{N}_k}\left\{\frac{\widehat{w}_k(\sigma)}{\tilde{w}_k(\sigma)} - 1\right\} \leq \epsilon_k; \qquad \text{(S2c)}$$

$$\|\mathbf{E}_{k-1,-}\| = \max_{\nu \in \Sigma_{k-1}}\left\{\left[\mathbf{E}_{k-1,-}\right]_{\nu,\nu}\right\} = \max_{\nu \in \Sigma_{k-1}}\left\{\frac{\tilde{w}_{k-1}^{-1}(\nu)}{\widehat{w}_{k-1}^{-1}(\nu)} - 1\right\} \leq \sqrt{\epsilon_{k-1}}; \qquad \text{(S2d)}$$

$$\max_{\nu \in \Sigma_{k-1}}\left\{\frac{\widehat{w}_{k-1}(\nu)}{\tilde{w}_{k-1}(\nu)} - 1\right\} \leq \epsilon_{k-1}. \qquad \text{(S2e)}$$

1

3. The net *changes on* $\mathbf{w}_k$ *and* $\mathbf{w}_{k-1}$ *are small*

$$\|\mathbf{E}_{k,+}^+ - \mathbf{E}_{k,-}^+\| = \max_{\sigma \in \mathfrak{N}_k} \left\{ \left| \frac{\widehat{w}_k^{1/2}(\sigma)}{w_k^{1/2}(\sigma)} - 1 \right| \right\} \le \sqrt{\epsilon_k'}; \tag{S3a}$$

$$\|\mathbf{E}_{k,+}^- - \mathbf{E}_{k,-}^-\| = \max_{\sigma \in \mathfrak{N}_k} \left\{ \left| \frac{w_k^{1/2}(\sigma)}{\widehat{w}_k^{1/2}(\sigma)} - 1 \right| \right\} \le \sqrt{\epsilon_k'}; \tag{S3b}$$

$$\max_{\sigma \in \mathfrak{N}_k} \left\{ \left| \frac{\widehat{w}_k(\sigma)}{w_k(\sigma)} - 1 \right| \right\} \le \epsilon_k'; \tag{S3c}$$

$$\|\mathbf{E}_{k-1,+} - \mathbf{E}_{k-1,-}\| = \max_{\nu \in \Sigma_{k-1}} \left\{ \left| \frac{w_{k-1}^{-1}(\nu)}{\widehat{w}_{k-1}^{-1}(\nu)} - 1 \right| \right\} \le \sqrt{\epsilon_{k-1}'}; \tag{S3d}$$

$$\max_{\nu \in \Sigma_{k-1}} \left\{ \left| \frac{\widehat{w}_{k-1}(\nu)}{w_{k-1}(\nu)} - 1 \right| \right\} \le \epsilon_{k-1}'. \tag{S3e}$$

A.2 Definitions of $\mathcal{L}_k$ and $\widehat{\mathcal{L}}_k$

Given a manifold $\mathcal{M}$ which is constructed by a series of connected sum, i.e., $\mathcal{M} = \mathcal{M}_1 \sharp \cdots \sharp \mathcal{M}_\kappa$. Let the Simplicial complex corresponding to $\mathcal{M}$ be $\mathrm{SC}_\ell = (\Sigma_0, \cdots, \Sigma_\ell)$, with the disjoint simplicial complex (of $\cup_{i=1}^\kappa \mathcal{M}_i$) being $\widehat{\mathrm{SC}}_\ell = (\widehat{\Sigma}_0, \cdots, \widehat{\Sigma}_\ell)$. For each k, the simplex sets can be decomposed into the following

$$\Sigma_k = \underbrace{\bigcup_{i=1}^\kappa \Sigma_k^{(i)}}_{\text{non-intersecting set:} \mathfrak{N}_k} \cup \underbrace{\bigcup_{j>i}^\kappa \Sigma_k^{(ij)+}}_{\text{created set:} \mathfrak{C}_k}.$$

Similarly,

$$\widehat{\Sigma}_k = \underbrace{\bigcup_{i=1}^\kappa \Sigma_k^{(i)}}_{\text{non-intersecting set:} \mathfrak{N}_k} \cup \underbrace{\bigcup_{j>i}^\kappa \Sigma_k^{(ij)-}}_{\text{destroyed set:} \mathfrak{D}_k}.$$

W.l.o.g., one can assume that the $(k-1)$-simplices set can be perfectly separated, i.e., $\mathfrak{C}_{k-1} = \mathfrak{D}_{k-1} = \emptyset$ (when analyzing the k-Laplacian). The above construction matches our intuition; by definition, a connected sum is a process of carving out a d-disk ($\mathfrak{D}_k$) and gluing two manifolds together ($\mathfrak{C}_k$).

We are interested in the perturbation of the k-Laplacian $\mathcal{L}_k$ w.r.t. the ideal (disjoint) Laplacian $\widehat{\mathcal{L}}_k$. Without carefully define both $\mathcal{L}_k$ and $\widehat{\mathcal{L}}_k$, the perturbation on the subspaces might be unbounded. With slight abuse of notation, we let $\mathbf{L} \leftarrow \mathcal{L}_k$, $\mathbf{L}_d \leftarrow \mathcal{L}_k^{\mathrm{down}}$, and $\mathbf{L}_u \leftarrow \mathcal{L}_k^{\mathrm{up}}$ (similar definitions for $\widehat{\mathcal{L}}$'s). The k is omitted and can be inferred from the context. The $\widehat{\mathbf{L}}$ and $\mathbf{L}$ are defined as follows. $\widehat{\mathbf{L}}$ is a block diagonal matrix, with the i-th (diagonal) block $\mathbf{L}^{(i)}$ described by $\mathcal{M}_i$ constructed from the sub-complex $\widehat{\mathrm{SC}}^{(i)}$ ($\widehat{\Sigma}_{k-1}^{(i)}$, $\widehat{\Sigma}_k^{(i)}$, and $\widehat{\Sigma}_{k+1}^{(i)}$). Due to manifolds being disjoint (i.e., $\cup_{i=1}^\kappa \mathcal{M}_i$), the Laplacian corresponding to such block, denoted $\widehat{\mathbf{L}}^{(i,i),(i,i)}$, will be a valid Laplacian. As for the intersecting k-simplices $\mathfrak{C}_k \cup \mathfrak{D}_k$, we let $\widehat{\mathbf{L}}^{(i,j),(k,l)} = \mathbf{L}^{(i,j),(k,l)}$ for all $ij, kl \in \binom{[k]}{2}$ so that the corresponding blocks of $\widehat{\mathbf{L}} - \mathbf{L}$ will be zero. Under this scenario, the unbounded increase of $(k+1)$-simplices caused by the intersecting k-simplices can be removed. Lastly, the off-diagonal blocks of $\widehat{\mathbf{L}}$ are set to zero. Specifically, $\widehat{\mathbf{L}}$ is,

2

$$\widehat{\mathbf{L}} = \left[\begin{array}{ccc|ccc|ccc}
\widehat{\mathbf{L}}^{(1,1),(1,1)} & & & & & & \widehat{\mathbf{L}}^{(1,1),(1,2)-} & \cdots & \widehat{\mathbf{L}}^{(1,1),(k-1,k)-} \\
& \ddots & & & \mathbf{0} & & \vdots & \ddots & \vdots \\
& & \widehat{\mathbf{L}}^{(k,k),(k,k)} & & & & \widehat{\mathbf{L}}^{(k,k),(1,2)-} & \cdots & \widehat{\mathbf{L}}^{(k,k),(k-1,k)-} \\
\hline
& & & \mathbf{L}^{(1,2)+,(1,2)+} & \cdots & \mathbf{L}^{(1,2)+,(k-1,k)+} & & & \\
& \mathbf{0} & & \vdots & \ddots & \vdots & & \mathbf{0} & \\
& & & \mathbf{L}^{(k-1,k)+,(1,2)+} & \cdots & \mathbf{L}^{(k-1,k)+,(k-1,k)+} & & & \\
\hline
\widehat{\mathbf{L}}^{(1,2)-,(1,1)} & \cdots & \widehat{\mathbf{L}}^{(1,2)-,(k,k)} & & & & \widehat{\mathbf{L}}^{(1,2)-,(1,2)-} & \cdots & \widehat{\mathbf{L}}^{(1,2)-,(k-1,k)-} \\
\vdots & \ddots & \vdots & & \mathbf{0} & & \vdots & \ddots & \vdots \\
\widehat{\mathbf{L}}^{(k-1,k)-,(1,1)} & \cdots & \widehat{\mathbf{L}}^{(k,k)-,(k,k)} & & & & \widehat{\mathbf{L}}^{(k-1,k)-,(1,2)-} & \cdots & \widehat{\mathbf{L}}^{(k-1,k)-,(k-1,k)-}
\end{array}\right].$$

Similarly, one can define $\mathbf{L}$ to be

$$\mathbf{L} = \left[\begin{array}{ccc|ccc|ccc}
\mathbf{L}^{(1,1),(1,1)} & & & \mathbf{L}^{(1,1),(1,2)+} & \cdots & \mathbf{L}^{(1,1),(k-1,k)+} & & & \\
& \ddots & & \vdots & \ddots & \vdots & & \mathbf{0} & \\
& & \mathbf{L}^{(k,k),(k,k)} & \mathbf{L}^{(k,k),(1,2)+} & \cdots & \mathbf{L}^{(k,k),(k-1,k)+} & & & \\
\hline
\mathbf{L}^{(1,2)+,(1,1)} & \cdots & \mathbf{L}^{(1,2)+,(k,k)} & \mathbf{L}^{(1,2)+,(1,2)+} & \cdots & \mathbf{L}^{(1,2)+,(k-1,k)+} & & & \\
\vdots & \ddots & \vdots & \vdots & \ddots & \vdots & & \mathbf{0} & \\
\mathbf{L}^{(k-1,k)+,(1,1)} & \cdots & \mathbf{L}^{(k,k)+,(k,k)} & \mathbf{L}^{(k-1,k)+,(1,2)+} & \cdots & \mathbf{L}^{(k-1,k)+,(k-1,k)+} & & & \\
\hline
& & & & & & \widehat{\mathbf{L}}^{(1,2)-,(1,2)-} & \cdots & \widehat{\mathbf{L}}^{(1,2)-,(k-1,k)-} \\
& \mathbf{0} & & & \mathbf{0} & & \vdots & \ddots & \vdots \\
& & & & & & \widehat{\mathbf{L}}^{(k-1,k)-,(1,2)-} & \cdots & \widehat{\mathbf{L}}^{(k-1,k)-,(k-1,k)-}
\end{array}\right].$$

Under this construction, the four lower right blocks, which correspond to the k-simplices in $\mathfrak{C}_k \cup \mathfrak{D}_k$, will be zero. If no new homology class is created/destroyed (Assumption 1) and the minimum eigenvalues of the last two diagonal blocks are bounded away from zero (Assumption 2), then the eigengap of $\mathbf{L}$ will simply be the minimum eigengap of each $\widehat{\mathbf{L}}^{(i)}$, i.e., $\mathrm{eigengap}(\mathbf{L}) = \min\{\delta_1, \cdots, \delta_\kappa\}$.

Now we formally define our formulation. Following the notations introduced in Section 3, and let $\mathcal{I}_\sigma$ be the index set of the k-simplex $\sigma \in \mathfrak{N}_k$ sampled from $\mathcal{M}_i$. Note that $\mathcal{I}_\sigma$ is defined only for $\sigma \in \mathfrak{N}_k$, which can be extended from the index set $\mathcal{I}_v$ for $v \in V$ introduced in Section 3 by $\mathcal{I}_\sigma = \{\sigma \in \mathfrak{N}_k : v \in \mathcal{I}_v \text{ for } v \in \sigma\}$. Note also that similar to $\mathcal{I}_v$ for V, $\mathcal{S}_\sigma$ can be larger than 1. For instance, if the manifold is constructed by gluing a torus (indexed by 1) and a circle (indexed by 2), then $\mathcal{S}_1 = \{1, 2\}$ and $\mathcal{S}_2 = \{3\}$; for an edge e belongs to the torus, we have $\mathcal{S}_{\mathcal{I}_e} = \{1, 2\}$. For every $\sigma \in \mathfrak{N}_k$, we write,

$$\sum_{\sigma \in \mathfrak{N}_k} \sum_{i \notin S_{\mathcal{I}_\sigma}} \mathbf{Y}_{\sigma,i}^2 \leq \sum_{\sigma \in \mathfrak{N}_k} \sum_{i=1}^{\beta_1} (\mathbf{Y}_{\sigma,i} - \widehat{\mathbf{Y}}_{\sigma,i})^2 \leq \sum_{\sigma \in \Sigma_k \cup \widehat{\Sigma}_k} \sum_{i=1}^{\beta_1} (\mathbf{Y}_{\sigma,i} - \widehat{\mathbf{Y}}_{\sigma,i})^2 = \|\mathbf{Y}\mathbf{O} - \widehat{\mathbf{Y}}\|_F^2.$$

3

Let $\text{DiffL}_k^{\text{down}} = \mathbf{L}_d - \widehat{\mathbf{L}}_d$ and $\text{DiffL}_k^{\text{up}} = \mathbf{L}_u - \widehat{\mathbf{L}}_u$, from [61] and the triangular inequality,

$$
\left\| \mathbf{Y}_{\mathfrak{N}_k,:} - \widehat{\mathbf{Y}}_{\mathfrak{N}_k,:} \right\|_F^2 = \sum_{\sigma \in \mathfrak{N}_k} \sum_{i \notin \mathcal{S}_{\mathcal{I}_\sigma}} \mathbf{Y}_{\sigma,i}^2 \leq \| \mathbf{Y} - \widehat{\mathbf{Y}} \mathbf{O} \|_F^2
$$

$$
\leq \frac{8 \cdot \min \left\{ \beta_k \left\| \mathbf{L} - \widehat{\mathbf{L}} \right\|^2, \| \mathbf{L} - \widehat{\mathbf{L}} \|_F^2 \right\}}{\min\{\delta_1, \cdots, \delta_\kappa\}}
$$

$$
\leq \frac{8 \cdot \min \left\{ \beta_k \left\| \text{DiffL}_k^{\text{down}} \right\|^2 + \beta_k \| \text{DiffL}_k^{\text{up}} \|^2, \| \text{DiffL}_k^{\text{down}} \|_F^2 + \| \text{DiffL}_k^{\text{up}} \|_F^2 \right\}}{\min\{\delta_1, \cdots, \delta_\kappa\}}
$$

$$
\overset{\dagger}{\leq} \frac{8\beta_k \left(\left\| \text{DiffL}_k^{\text{down}} \right\|^2 + \| \text{DiffL}_k^{\text{up}} \|^2 \right)}{\min\{\delta_1, \cdots, \delta_\kappa\}}.
$$

Remark. The bound w.r.t. the Frobenius norm is omitted (the last inequality $\dagger$) based on two reasons: (i) $\mathcal{L}_k$ has complicated forms for large k, therefore, it is hard to derive a concise expression; and (ii) $\| \cdot \|_F$ is usually larger than $\beta_k \| \cdot \|$.

A.3 Useful lemmas

Here we omit the k for $\mathfrak{N}$, $\mathfrak{C}$, and $\mathfrak{D}$ for simplicity. Let $\lambda_k = \| \mathcal{L}_k \|$ be the bound on the spectral norm of k-Laplacian. Here, $\lambda_k = k + 2$ for $\mathcal{L}$'s built from simplicial complexes; $\lambda_k = 2k + 2$ for those built from cubical complexes (see also Proposition S3). The following two lemmas bound the effects of $\mathcal{E}_{k,+}$, $\mathcal{E}_{k,-}$, $\mathcal{E}_{k+1,+}$, and $\mathcal{E}_{k+1,-}$ in their changes to the weights ($\mathbf{W}_k$ and $\mathbf{W}_{k-1}$) of the k and $(k-1)$-simplices; we will find them useful in proving Theorem 1.

Lemma S1. *Let* $\mathbf{W}_k$, $\widehat{\mathbf{W}}_k$, $\mathcal{E}_{k,+}$, *and* $\mathcal{E}_{k,-}$ *defined in Assumption S1, we have*

$$
\left\| \mathcal{E}_{k,+} \mathbf{B}_k^\top \mathbf{W}_{k-1}^{-1} \mathbf{B}_k \mathcal{E}_{k,+} \right\| \leq \lambda_{k-1} \epsilon_{k-1},
$$

$$
\left\| \mathcal{E}_{k,-} \mathbf{B}_k^\top \widehat{\mathbf{W}}_{k-1}^{-1} \mathbf{B}_k \mathcal{E}_{k,-} \right\| \leq \lambda_{k-1} \epsilon_{k-1}.
$$

Proof. We first inspect the case of $\mathfrak{C}$, i.e., the first equation involving $\mathcal{E}_{k,+}$,

$$
[\mathcal{E}_{k,+}]_{\sigma,\sigma} = \begin{cases} w_k^{1/2}(\sigma) & \text{if } \sigma \in \mathfrak{C}; \\ 0 & \text{otherwise.} \end{cases}
$$

for any $\nu \in \Sigma_{k-1}$, we have,

$$
w_{k-1}(\nu) = |\mathbf{B}_k(\nu)| \mathbf{w}_k;
$$
$$
\tilde{w}_{k-1}(\nu) = |\mathbf{B}_k(\nu)| \tilde{\mathbf{w}}_k.
$$

Therefore,

$$
\epsilon_{k-1} w_{k-1}(\nu) \geq \epsilon_{k-1} \tilde{w}_{k-1}(\nu) \geq w_{k-1}(\nu) - \tilde{w}_{k-1}(\nu) = |\mathbf{B}_k(\nu)| (\mathbf{w}_k - \tilde{\mathbf{w}}_k)
$$
$$
= |\mathbf{B}_k(\nu)| [\tilde{\mathbf{w}}_k \mathbf{E}_k + \mathcal{E}_{k,+}] \geq |\mathbf{B}_k(\nu)| \mathcal{E}_{k,+} = \deg(\nu).
$$

Let f_m be the k-eigencochain corresponding to the largest eigenvalue of $\mathcal{E}_{k,+} \mathbf{B}_k^\top \mathbf{W}_{k-1}^{-1} \mathbf{B}_k \mathcal{E}_{k,+}$. From Eq. (3.6) of [26], we have,

$$
\| \mathcal{E}_{k,+} \mathbf{B}_k^\top \mathbf{W}_{k-1}^{-1} \mathbf{B}_k \mathcal{E}_{k,+} \|_2 \leq \| \mathbf{L}_d \| \cdot \frac{\sum_{\nu \in \Sigma_{k-1}} f_m^2(\nu) \deg(\nu)}{\sum_{\nu \in \Sigma_{k-1}} f_m^2(\nu) w_{k-1}(\nu)}
$$

$$
\leq \lambda_{k-1} \epsilon_{k-1} \cdot \frac{\sum_{\nu \in \Sigma_{k-1}} f_m^2(\nu) w_{k-1}(\nu)}{\sum_{\nu \in \Sigma_{k-1}} f_m^2(\nu) w_{k-1}(\nu)} = \lambda_{k-1} \epsilon_{k-1}.
$$

4

The case of $\mathfrak{D}$ follows similarly. ∎

The following lemma bounds the changes in $(k+1)$-simplices with ϵ_k.

Lemma S2. *Let* $\mathbf{W}$ *be either* $\mathbf{W}_k$ *or* $\widehat{\mathbf{W}}_k$, *and* $\boldsymbol{\mathcal{E}}$ *be either* $\boldsymbol{\mathcal{E}}_{k+1,+}$ *or* $\boldsymbol{\mathcal{E}}_{k+1,-}$ *defined in Assumption S1, we have*

$$\left\| \mathbf{W}\mathbf{B}_{k+1}\boldsymbol{\mathcal{E}}\mathbf{B}_{k+1}^\top\mathbf{W} \right\| \leq \lambda_k\epsilon_k.$$

Proof. Consider the case of $\mathbf{W}_k$ and $\boldsymbol{\mathcal{E}}_{k+1,+}$. For any $\sigma \in \Sigma_k$,

$$w_k(\sigma) = |\mathbf{B}_{k+1}(\sigma)|\mathbf{w}_{k+1};$$
$$\tilde{w}_k(\sigma) = |\mathbf{B}_{k+1}(\sigma)|\tilde{\mathbf{w}}_{k+1}.$$

Therefore, for any $\sigma \in \mathfrak{N}$ (do not count the one in $\boldsymbol{\mathcal{E}}_{k,\pm}$) we have,

$$\epsilon_k w_k(\sigma) \geq \epsilon_k \tilde{w}_k(\sigma) \geq w_k(\sigma) - \tilde{w}(\sigma) = |\mathbf{B}_{k+1}(\sigma)|(\mathbf{w}_{k+1} - \tilde{\mathbf{w}}_{k+1}) = |\mathbf{B}_{k+1}(\sigma)|\boldsymbol{\mathcal{E}}_{k+1,+}.$$

Let f_m be the k-eigencochain corresponding to the largest eigenvalue of the matrix $\mathbf{W}_k^{-1/2}\mathbf{B}_{k+1}\boldsymbol{\mathcal{E}}_{k+1,+}\mathbf{B}_{k+1}^\top\mathbf{W}_k^{-1/2}$. From Eq. (3.6) of [26],

$$\left\| \mathbf{W}_k^{-1/2}\mathbf{B}_{k+1}\boldsymbol{\mathcal{E}}_{k+1,+}\mathbf{B}_{k+1}^\top\mathbf{W}_k^{-1/2} \right\| \leq (k+2) \cdot \frac{\sum_{\sigma\in\mathfrak{N}} f_m^2(\sigma)\deg(\sigma)}{\sum_{\sigma\in\mathfrak{N}} f_m^2(\sigma)w_k(\sigma)}$$

$$\leq \lambda_k\epsilon_k \frac{\sum_{\sigma\in\mathfrak{N}} f_m^2(e)w_k(e)}{\sum_{\sigma\in\mathfrak{N}} f_m^2(e)w_k(e)} = \lambda_k\epsilon_k$$

Here $\deg(\sigma) = |\mathbf{B}_{k+1}(\sigma)\mathrm{diag}(\boldsymbol{\mathcal{E}}_{k+1,+})|$. Consider the case when $\mathbf{W} \leftarrow \widehat{\mathbf{W}}_k$ and $\boldsymbol{\mathcal{E}} \leftarrow \boldsymbol{\mathcal{E}}_{k+1,+}$, we have,

$$\epsilon_k \widehat{w}_k(\sigma) \geq \epsilon_k \tilde{w}_k(\sigma) \geq w_k(\sigma) - \tilde{w}(\sigma) = |\mathbf{B}_{k+1}(\sigma)|(\mathbf{w}_{k+1} - \tilde{\mathbf{w}}_{k+1}) = |\mathbf{B}_{k+1}(\sigma)|\boldsymbol{\mathcal{E}}_{k+1,+}.$$

The result follows similarly for $\boldsymbol{\mathcal{E}} \leftarrow \boldsymbol{\mathcal{E}}_{k+1,-}$; this completes the proof. ∎

A.4 Proof of Theorem 1

Now we start the formal proof of Theorem 1. We will break the proof into two parts, i.e., the *down* and *up* parts involving $\mathrm{DiffL}_k^{\mathrm{down}}$ and $\mathrm{DiffL}_k^{\mathrm{up}}$, respectively.

Proof of the $\mathrm{DiffL}_k^{\mathrm{down}}$ **term in Theorem 1.** The explicit form of the *down* Laplacian can be written as

$$\widehat{\mathbf{L}}_d = \begin{bmatrix} \mathbf{M}_{\mathfrak{N}}\widehat{\mathbf{W}}_k^{1/2}\mathbf{B}_k^\top\widehat{\mathbf{W}}_{k-1}^{-1}\mathbf{B}_k\widehat{\mathbf{W}}_k^{1/2}\mathbf{M}_{\mathfrak{N}} & \mathbf{0} & \mathbf{M}_{\mathfrak{N}}\widehat{\mathbf{W}}_k^{1/2}\mathbf{B}_k^\top\widehat{\mathbf{W}}_{k-1}^{-1}\mathbf{B}_k\boldsymbol{\mathcal{E}}_{k,-}^{1/2}\mathbf{M}_{\mathfrak{D}} \\ \mathbf{0} & \mathbf{M}_{\mathfrak{C}}\boldsymbol{\mathcal{E}}_{k,+}^{1/2}\mathbf{B}_k^\top\mathbf{W}_{k-1}^{-1}\mathbf{B}_k\boldsymbol{\mathcal{E}}_{k,+}^{1/2}\mathbf{M}_{\mathfrak{C}} & \mathbf{0} \\ \mathbf{M}_{\mathfrak{D}}\boldsymbol{\mathcal{E}}_{k,-}^{1/2}\mathbf{B}_k^\top\widehat{\mathbf{W}}_{k-1}^{-1}\mathbf{B}_k\widehat{\mathbf{W}}_k^{1/2}\mathbf{M}_{\mathfrak{N}} & \mathbf{0} & \mathbf{M}_{\mathfrak{D}}\boldsymbol{\mathcal{E}}_{k,-}^{1/2}\mathbf{B}_k^\top\widehat{\mathbf{W}}_{k-1}^{-1}\mathbf{B}_k\boldsymbol{\mathcal{E}}_{k,-}^{1/2}\mathbf{M}_{\mathfrak{D}} \end{bmatrix}.$$

And,

$$\mathbf{L}_d = \begin{bmatrix} \mathbf{M}_{\mathfrak{N}}\mathbf{W}_k^{1/2}\mathbf{B}_k^\top\mathbf{W}_{k-1}^{-1}\mathbf{B}_k\mathbf{W}_k^{1/2}\mathbf{M}_{\mathfrak{N}} & \mathbf{M}_{\mathfrak{N}}\mathbf{W}_k^{1/2}\mathbf{B}_k^\top\mathbf{W}_{k-1}^{-1}\mathbf{B}_k\boldsymbol{\mathcal{E}}_{k,+}^{1/2}\mathbf{M}_{\mathfrak{C}} & \mathbf{0} \\ \mathbf{M}_{\mathfrak{C}}\boldsymbol{\mathcal{E}}_{k,+}^{1/2}\mathbf{B}_k^\top\mathbf{W}_{k-1}^{-1}\mathbf{B}_k\mathbf{W}_k^{1/2}\mathbf{M}_{\mathfrak{N}} & \mathbf{M}_{\mathfrak{C}}\boldsymbol{\mathcal{E}}_{k,+}^{1/2}\mathbf{B}_k^\top\mathbf{W}_{k-1}^{-1}\mathbf{B}_k\boldsymbol{\mathcal{E}}_{k,+}^{1/2}\mathbf{M}_{\mathfrak{C}} & \mathbf{0} \\ \mathbf{0} & \mathbf{0} & \mathbf{M}_{\mathfrak{D}}\boldsymbol{\mathcal{E}}_{k,-}^{1/2}\mathbf{B}_k^\top\widehat{\mathbf{W}}_{k-1}^{-1}\mathbf{B}_k\boldsymbol{\mathcal{E}}_{k,-}^{1/2}\mathbf{M}_{\mathfrak{D}} \end{bmatrix}.$$

5

Here, $\mathbf{M}_{\mathfrak{N}}$, $\mathbf{M}_{\mathfrak{C}}$, and $\mathbf{M}_{\mathfrak{D}}$ are diagonal masks for k-simplex sets $\mathfrak{N}$, $\mathfrak{C}$, and $\mathfrak{D}$, respectively. By triangular inequality,

$$
\left\| \mathbf{L}_d - \widehat{\mathbf{L}}_d \right\| \leq \underbrace{\left\| \mathbf{M}_{\mathfrak{N}} \mathbf{W}_k^{1/2} \mathbf{B}_k^\top \mathbf{W}_{k-1}^{-1} \mathbf{B}_k \mathbf{W}_k^{1/2} \mathbf{M}_{\mathfrak{N}} - \mathbf{M}_{\mathfrak{N}} \widehat{\mathbf{W}}_k^{1/2} \mathbf{B}_k^\top \widehat{\mathbf{W}}_{k-1}^{-1} \mathbf{B}_k \widehat{\mathbf{W}}_k^{1/2} \mathbf{M}_{\mathfrak{N}} \right\|}_{(*)} +
$$

$$
2 \left[\underbrace{\left\| \mathbf{M}_{\mathfrak{N}} \mathbf{W}_k^{1/2} \mathbf{B}_k^\top \mathbf{W}_{k-1}^{-1} \mathbf{B}_k \boldsymbol{\mathcal{E}}_{k,+}^{1/2} \mathbf{M}_{\mathfrak{C}} \right\|}_{(\dagger)} + \left\| \mathbf{M}_{\mathfrak{N}} \widehat{\mathbf{W}}_k^{1/2} \mathbf{B}_k^\top \widehat{\mathbf{W}}_{k-1}^{-1} \mathbf{B}_k \boldsymbol{\mathcal{E}}_{k,-}^{1/2} \mathbf{M}_{\mathfrak{D}} \right\| \right].
$$

$$(\text{S4})$$

Expand the $\mathbf{W}_k$ with $\widehat{\mathbf{W}}_k$ and omit $\mathbf{M}_{\mathfrak{N}}$ for simplicity, the first term of (S4) can be bounded by

$$
(*) \leq \left\| \widehat{\mathbf{W}}_k^{1/2} \left(\mathbf{I} + (\mathbf{E}_{k,+}^+ - \mathbf{E}_{k,-}^+) \right) \mathbf{B}_k^\top \widehat{\mathbf{W}}_{k-1}^{-1} \left(\mathbf{I} - (\mathbf{E}_{k-1,+} - \mathbf{E}_{k-1,-}) \right) \mathbf{B}_k \widehat{\mathbf{W}}_k^{1/2} \left(\mathbf{I} + (\mathbf{E}_{k,+}^+ - \mathbf{E}_{k,-}^+) \right) \right.
$$

$$
\left. - \widehat{\mathbf{W}}_k^{1/2} \mathbf{B}_k^\top \widehat{\mathbf{W}}_{k-1}^{-1} \mathbf{B}_k \widehat{\mathbf{W}}_k^{1/2} \right\|
$$

$$
\leq \left[\left(\left\| 2 \cdot (\mathbf{E}_{k,+}^+ - \mathbf{E}_{k,-}^+) \right\| + \left\| (\mathbf{E}_{k,+}^+ - \mathbf{E}_{k,-}^+)^2 \right\| \right) \cdot \left\| \widehat{\mathbf{L}}_d \right\| + \right.
$$

$$
\left. \left(1 + \sqrt{\epsilon_k'} \right)^2 \left\| \widehat{\mathbf{W}}_k^{1/2} \mathbf{B}_k^\top \widehat{\mathbf{W}}_{k-1}^{-1} (\mathbf{E}_{k-1,+} - \mathbf{E}_{k-1,-}) \mathbf{B}_k \widehat{\mathbf{W}}_k^{1/2} \right\| \right]
$$

$$
\leq \left[\left\| 2 \cdot (\mathbf{E}_{k,+}^+ - \mathbf{E}_{k,-}^+) \right\| + \left\| (\mathbf{E}_{k,+}^+ - \mathbf{E}_{k,-}^+)^2 \right\| + \left(1 + \sqrt{\epsilon_k'} \right)^2 \left\| \mathbf{E}_{k-1,+} - \mathbf{E}_{k-1,-} \right\| \right] \cdot \left\| \widehat{\mathbf{L}}_d \right\|
$$

$$
\overset{*}{\leq} \left[2\sqrt{\epsilon_k'} + \epsilon_k' + \left(1 + \sqrt{\epsilon_k'} \right)^2 \sqrt{\epsilon_{k-1}'} \right] \cdot \left\| \tilde{\mathbf{L}}_d \right\|.
$$

The last two terms of (S4) can be bounded using Lemma S1, i.e.,

$$
(\dagger) = \left\| \mathbf{M}_{\mathfrak{N}} \mathbf{W}_k^{1/2} \mathbf{B}_k^\top \mathbf{W}_{k-1}^{-1} \mathbf{B}_k \boldsymbol{\mathcal{E}}_{k,+}^{1/2} \mathbf{M}_{\mathfrak{C}} \right\| \leq \left\| \mathbf{M}_{\mathfrak{N}} \mathbf{W}_k^{1/2} \mathbf{B}_k^\top \mathbf{W}_{k-1}^{-1/2} \right\| \cdot \left\| \mathbf{W}_{k-1}^{-1/2} \mathbf{B}_k \boldsymbol{\mathcal{E}}_{k,+}^{1/2} \mathbf{M}_{\mathcal{I}} \right\|
$$

$$
\leq \left\| \mathbf{L}_d \right\| \sqrt{\epsilon_{k-1}}.
$$

The last term of (S4) can also be bounded by $\|\tilde{\mathbf{L}}_d\| \sqrt{\epsilon_{k-1}}$ using Lemma S1. Since $\|\mathbf{L}_d\|$, $\left\| \widehat{\mathbf{L}}_d \right\|$, and $\left\| \tilde{\mathbf{L}}_d \right\|$ have the same upper bound λ_{k-1}, we have

$$
\left\| \mathbf{L}_d - \widehat{\mathbf{L}}_d \right\|^2 \leq \left[2\sqrt{\epsilon_k'} + \epsilon_k' + \left(1 + \sqrt{\epsilon_k'} \right)^2 \sqrt{\epsilon_{k-1}'} + 4\sqrt{\epsilon_{k-1}} \right]^2 \lambda_{k-1}^2.
$$

$$\blacksquare$$

Proof of the $\mathsf{DiffL}_k^{\mathrm{up}}$ **term in Theorem 1.** The explicit form of $\widehat{\mathbf{L}}_u$ is,

$$
\widehat{\mathbf{L}}_u = \left[\begin{array}{c|c|c} \mathbf{M}_{\mathfrak{N}} \widehat{\mathbf{W}}_k^{-1/2} \mathbf{B}_{k+1} \widehat{\mathbf{W}}_{k+1} \mathbf{B}_{k+1}^\top \widehat{\mathbf{W}}_k^{-1/2} \mathbf{M}_{\mathfrak{N}} & \mathbf{0} & \mathbf{M}_{\mathfrak{N}} \widehat{\mathbf{W}}_k^{-1/2} \mathbf{B}_{k+1} \widehat{\mathbf{W}}_{k+1} \mathbf{B}_{k+1}^\top \boldsymbol{\mathcal{E}}_{k,-}^{1/2} \mathbf{M}_{\mathfrak{D}} \\ \hline \mathbf{0} & \mathbf{M}_{\mathfrak{C}} \boldsymbol{\mathcal{E}}_{k,+}^{-1/2} \mathbf{B}_{k+1} \mathbf{W}_{k+1} \mathbf{B}_{k+1}^\top \boldsymbol{\mathcal{E}}_{k,+}^{-1/2} \mathbf{M}_{\mathfrak{C}} & \mathbf{0} \\ \hline \mathbf{M}_{\mathfrak{D}} \boldsymbol{\mathcal{E}}_{k,-}^{-1/2} \mathbf{B}_{k+1} \widehat{\mathbf{W}}_{k+1} \mathbf{B}_{k+1}^\top \widehat{\mathbf{W}}_k^{-1/2} \mathbf{M}_{\mathfrak{N}} & \mathbf{0} & \mathbf{M}_{\mathfrak{D}} \boldsymbol{\mathcal{E}}_{k,-}^{-1/2} \mathbf{B}_{k+1} \widehat{\mathbf{W}}_{k+1} \mathbf{B}_{k+1}^\top \boldsymbol{\mathcal{E}}_{k,+}^{-1/2} \mathbf{M}_{\mathfrak{D}} \end{array} \right].
$$

And,

6

$$\mathbf{L}_u = \left[\begin{array}{cc|c} \mathbf{M}_\mathfrak{N}\mathbf{W}_k^{-1/2}\mathbf{B}_{k+1}\mathbf{W}_{k+1}\mathbf{B}_{k+1}^\top\mathbf{W}_k^{-1/2}\mathbf{M}_\mathfrak{N} & \mathbf{M}_\mathfrak{N}\mathbf{W}_k^{-1/2}\mathbf{B}_{k+1}\mathbf{W}_{k+1}\mathbf{B}_{k+1}^\top\boldsymbol{\mathcal{E}}_{k,+}^{1/2}\mathbf{M}_\mathfrak{C} & \mathbf{0} \\ \hline \mathbf{M}_\mathfrak{C}\boldsymbol{\mathcal{E}}_{k,+}^{-1/2}\mathbf{B}_{k+1}\mathbf{W}_{k+1}\mathbf{B}_{k+1}^\top\mathbf{W}_k^{-1/2}\mathbf{M}_\mathfrak{N} & \mathbf{M}_\mathfrak{C}\boldsymbol{\mathcal{E}}_{k,+}^{-1/2}\mathbf{B}_{k+1}\mathbf{W}_{k+1}\mathbf{B}_{k+1}^\top\boldsymbol{\mathcal{E}}_{k,+}^{-1/2}\mathbf{M}_\mathfrak{C} & \mathbf{0} \\ \hline \mathbf{0} & \mathbf{0} & \mathbf{M}_\mathfrak{D}\boldsymbol{\mathcal{E}}_{k,-}^{-1/2}\mathbf{B}_{k+1}\widehat{\mathbf{W}}_{k+1}\mathbf{B}_{k+1}^\top\boldsymbol{\mathcal{E}}_{k,+}^{-1/2}\mathbf{M}_\mathfrak{D} \end{array}\right].$$

The perturbation is,

$$\left\|\mathbf{L}_u - \widehat{\mathbf{L}}_u\right\| \leq \underbrace{\left\|\mathbf{M}_\mathfrak{N}\mathbf{W}_k^{-1/2}\mathbf{B}_{k+1}\mathbf{W}_{k+1}\mathbf{B}_{k+1}^\top\mathbf{W}_k^{-1/2}\mathbf{M}_\mathfrak{N} - \mathbf{M}_\mathfrak{N}\widehat{\mathbf{W}}_k^{-1/2}\mathbf{B}_{k+1}\widehat{\mathbf{W}}_{k+1}\mathbf{B}_{k+1}^\top\widehat{\mathbf{W}}_k^{-1/2}\mathbf{M}_\mathfrak{N}\right\|}_{(*)} +$$

$$2\left[\underbrace{\left\|\mathbf{M}_\mathfrak{N}\mathbf{W}_k^{-1/2}\mathbf{B}_{k+1}\mathbf{W}_{k+1}\mathbf{B}_{k+1}^\top\boldsymbol{\mathcal{E}}_{k,+}^{1/2}\mathbf{M}_\mathfrak{C}\right\|}_{(\dagger)} + \left\|\mathbf{M}_\mathfrak{N}\widehat{\mathbf{W}}_k^{-1/2}\mathbf{B}_{k+1}\widehat{\mathbf{W}}_{k+1}\mathbf{B}_{k+1}^\top\boldsymbol{\mathcal{E}}_{k,-}^{1/2}\mathbf{M}_\mathfrak{D}\right\|\right].$$
$$(S5)$$

The first term of (S5) can be bounded by expanding $\mathbf{W}_{k+1}$ w.r.t. $\widehat{\mathbf{W}}_{k+1}$, i.e., $\mathbf{W}_{k+1} = \widehat{\mathbf{W}}_{k+1} + (\boldsymbol{\mathcal{E}}_{k+1,+} - \boldsymbol{\mathcal{E}}_{k+1,-})$. As slight abuse of notation, we let $\mathbf{W}_k \leftarrow \mathbf{W}_k[\mathfrak{N}, \mathfrak{N}]$, $\mathbf{B}_{k+1} \leftarrow \mathbf{B}_{k+1}[\mathfrak{N}, :]$. The first term $(*)$ of (S5) becomes

$$(*) \leq \left\|\mathbf{W}_k^{-1/2}\mathbf{B}_{k+1}\widehat{\mathbf{W}}_{k+1}\mathbf{B}_{k+1}^\top\mathbf{W}_k^{-1/2} - \widehat{\mathbf{W}}_k^{-1/2}\mathbf{B}_{k+1}\widehat{\mathbf{W}}_{k+1}\mathbf{B}_{k+1}^\top\widehat{\mathbf{W}}_k^{-1/2}\right\|$$

$$\leq \left\|\mathbf{W}_k^{-1/2}\mathbf{B}_{k+1}\widehat{\mathbf{W}}_{k+1}\mathbf{B}_{k+1}^\top\mathbf{W}_k^{-1/2} - \widehat{\mathbf{W}}_k^{-1/2}\mathbf{B}_{k+1}\widehat{\mathbf{W}}_{k+1}\mathbf{B}_{k+1}^\top\widehat{\mathbf{W}}_k^{-1/2}\right\| +$$

$$\left\|\mathbf{W}_k^{-1/2}\mathbf{B}_{k+1}\boldsymbol{\mathcal{E}}_{k+1,+}\mathbf{B}_{k+1}^\top\mathbf{W}_k^{-1/2} - \widehat{\mathbf{W}}_k^{-1/2}\mathbf{B}_{k+1}\boldsymbol{\mathcal{E}}_{k+1,-}\mathbf{B}_{k+1}^\top\widehat{\mathbf{W}}_k^{-1/2}\right\|$$

$$\overset{\ddagger}{\leq} \left(2\|\mathbf{E}_{k,+}^- - \mathbf{E}_{k,-}^-\| + \left\|\left(\mathbf{E}_{k,+}^- - \mathbf{E}_{k,-}^-\right)^2\right\|\right) \cdot \left\|\widehat{\mathbf{L}}_u\right\| +$$

$$\left\|\mathbf{W}_k^{-1/2}\mathbf{B}_{k+1}\boldsymbol{\mathcal{E}}_{k+1,+}\mathbf{B}_{k+1}^\top\mathbf{W}_k^{-1/2} - \widehat{\mathbf{W}}_k^{-1/2}\mathbf{B}_{k+1}\boldsymbol{\mathcal{E}}_{k+1,-}\mathbf{B}_{k+1}^\top\widehat{\mathbf{W}}_k^{-1/2}\right\|$$

$$\overset{\S}{\leq} \left[2\sqrt{\epsilon_k'} + \epsilon_k' + 2\epsilon_k\right]\lambda_k$$

The $\ddagger$ term holds by expanding $\mathbf{W}_k^{-1/2} = \widehat{\mathbf{W}}_1^{-1/2}\left(\mathbf{I} - (\mathbf{E}_{k,+}^- - \mathbf{E}_{k,-}^-)\right)$ and following a similar approach of the *down* Laplacian. The $\S$ term holds by bounding $\mathbf{E}_{k,+}^- - \mathbf{E}_{k,-}^-$ with Assumption S1 (ϵ_k') and using Lemma S2 (ϵ_k).

The $(\dagger)$ term in (S5) can be bounded by ϵ_k using Lemma S2, i.e.,

$$(\dagger) \overset{\ddagger}{=} \left\|\mathbf{M}_\mathfrak{N}\mathbf{W}_k^{-1/2}\mathbf{B}_{k+1}\boldsymbol{\mathcal{E}}_{k+1,+}\mathbf{B}_{k+1}^\top\boldsymbol{\mathcal{E}}_{k,+}^{-1/2}\mathbf{M}_\mathfrak{C}\right\|$$

$$\leq \left\|\mathbf{M}_\mathfrak{N}\mathbf{W}_k^{-1/2}\mathbf{B}_{k+1}\boldsymbol{\mathcal{E}}_{k+1,+}^{1/2}\right\| \cdot \left\|\boldsymbol{\mathcal{E}}_{k+1,+}^{1/2}\mathbf{B}_{k+1}^\top\boldsymbol{\mathcal{E}}_{k,+}^{-1/2}\right\|$$

$$\leq \sqrt{\lambda_k\epsilon_k} \cdot \left\|\boldsymbol{\mathcal{E}}_{k+1,+}^{1/2}\mathbf{B}_{k+1}^\top\boldsymbol{\mathcal{E}}_{k,+}^{-1/2}\right\|$$

$$\overset{\S}{\leq} \sqrt{\epsilon_k}\lambda_k.$$

$\ddagger$ holds because the intersection of triangles of $\boldsymbol{\mathcal{E}}_{k,+}$, and $\mathbf{W}_k$ is the triangles with non-zero entries in $\boldsymbol{\mathcal{E}}_{k+1,+}$. $\S$ holds (the $\sqrt{\lambda_k}$ term) because $\boldsymbol{\mathcal{E}}_{k+1,+}^{1/2}\mathbf{B}_{k+1}^\top\boldsymbol{\mathcal{E}}_{k,+}^{-1/2}$ is a submatrix of $\mathbf{W}_{k+1}^{1/2}\mathbf{B}_{k+1}^\top\mathbf{W}_k^{-1/2}$; hence, the spectral norm will be upper bounded by the *up* Laplacian $\|\mathbf{L}_u\| \leq \lambda_k$.

7

Therefore, we have

$$\left\| \mathbf{L}_u - \widehat{\mathbf{L}}_u \right\|^2 \leq \left[2\sqrt{\epsilon'_k} + \epsilon'_k + 2\epsilon_k + 4\sqrt{\epsilon_k} \right]^2 \lambda_k^2.$$

Combining the bound involving $\mathsf{DiffL}_k^{\mathrm{down}}$ completes the proof of Theorem 1. ∎

B Proofs of propositions in Applications (Section 5)

B.1 Proof of Proposition 3: the properties of the induced digraph

The proof is based on the convenient properties of the harmonic flow (the basis of the homology vector space), i.e., they are both *divergence-free* and *curl-free* [12, 35, 48].

Proof of Proposition 3. **Reachable:** the harmonic flow is divergence free, indicating that the incoming flow must be equal to the outgoing flow. If there exists a vertex that is not *reachable* to itself, then this vertex will either be a *source* or *sink* in the digraph. It violates the assumption that the flow is divergence free. Therefore such vertex will not exist.

No short-circuiting: the harmonic flow is curl free; from Stoke's theorem (or Poincaré Lemma [33]), we have that any path-integral travel along any homology class will be a constant. If there exists a loop such that it does not traverse along with any homology class, the loop integral along this cycle will be zero (by Stoke's theorem). By assumption, the path-integral will always be positive. To generate a loop whose integral is zero, one has to travel "upward" in the digraph; this violates the assumption that we are finding a cycle in the digraph, implying that every loop will traverse along at least one homology class. ∎

B.2 Proof of Proposition 4: $\mathcal{H}_1$ embedding of $\mathbb{T}^m$

The proof is based on the fact that each harmonic 1-form of the flat m-(flat) torus can be expressed as the m-dimensional standard basis multiplied with some intensities in the intrinsic coordinate. The closed-form of the upper bound of the embedding distribution in any direction can be derived using the (high-dimensional) polar coordinate system, indicating that the envelope is an m-dimensional ellipsoid. The detailed proof is provided below.

Proof of Proposition 4. The harmonic vector field in an m-flat torus $\mathbb{T}^m$ is a constant in each coordinate, i.e., $\mathbf{v} = [v_1, \cdots, v_m] \in \mathbb{R}^m$. The manifold $\mathbb{T}^m$ is an m-dimensional cube with the periodic boundary condition, i.e., $0 = 2\pi$. From [12, 59], the edge flow $\boldsymbol{\omega}_e$ for an edge $e = (i, j) \in E$ can be written exactly as a linear map, i.e.,

$$\omega_e = \int_0^1 \mathbf{v}^\top(\boldsymbol{\gamma}(t))\gamma'(t)\mathrm{d}t = \int_0^1 [\mathbf{v}(\mathbf{x}_i) + (\mathbf{v}(\mathbf{x}_j) - \mathbf{v}(\mathbf{x}_i))t]^\top (\mathbf{x}_j - \mathbf{x}_i)\mathrm{d}t$$

$$= \frac{1}{2}(\mathbf{v}(\mathbf{x}_i) + \mathbf{v}(\mathbf{x}_j))^\top (\mathbf{x}_j - \mathbf{x}_i)$$

Where $\boldsymbol{\gamma}(t)$ is the geodesic on $\mathcal{M}$ connecting $\mathbf{x}_i$ and $\mathbf{x}_j$ with $\boldsymbol{\gamma}(0) = \mathbf{x}_i$ and $\boldsymbol{\gamma}(1) = \mathbf{x}_j$. Any point $\mathbf{x} \in \mathbb{R}^m$, with $r = \|\mathbf{x}\|$, can be written as $\mathbf{x} = [rf_1(\boldsymbol{\Phi}), rf_2(\boldsymbol{\Phi}), \cdots, rf_m(\boldsymbol{\Phi})]$, where $\boldsymbol{\Phi} \in \mathbb{R}^{m-1}$ is the high-dimensional polar coordinate; for instance, a point in 2D is $[r\cos(\theta), r\sin(\theta)]$ with $\boldsymbol{\Phi} = [\theta]$, while a point in 3D having $\boldsymbol{\Phi} = [\theta, \varphi]$ is $[r\cos\varphi\sin\theta, r\sin\varphi\sin\theta, r\cos\theta]$. The conditional distribution given a fixed $\boldsymbol{\Phi}$ is simply the distribution of edge lengths, i.e., $p(rv_1f_1, \cdots, rv_mf_m|\boldsymbol{\Phi}) = p(r)$. Since $p(r)$ is bounded by some constant δ representing the maximum edge length, the envelope of the distribution is bounded by $[\delta v_1 f_1(\boldsymbol{\Phi}), \cdots, \delta v_m f_m(\boldsymbol{\Phi})]$, indicating that it is an m-ellipsoid with the length of the i-th semi-axes being δv_i. ∎

C The maximum eigenvalue of $\mathcal{L}_k$ constructed from a cubical complex

In this section, we would like to show the bound on the spectral norm of $\mathcal{L}_k$ built from a cubical complex. The property is found useful in extending Theorem 1 to Corollary 2; namely, the goal is

8

to show that $\|\mathcal{L}_k\|_2 \leq \lambda_k = (2k+2)$. Note that $\|\mathcal{L}_k^{\text{down}}\| = \|\mathbf{A}_k^\top \mathbf{A}_k\| = \|\mathbf{A}_k \mathbf{A}_k^\top\| = \|\mathcal{L}_{k-1}^{\text{up}}\|$. W.l.o.g., one can inspect only the up-Laplacian. We provide the following proposition that is largely based on the similar analysis [26] of $\|\mathcal{L}_k\|$ for SC.

Proposition S3. *Given an* up k-*Laplacian* $\mathcal{L}_k^{\text{up}} = \mathbf{A}_{k+1}\mathbf{A}_{k+1}^\top$ *with* $\mathbf{A}_{k+1} = \mathbf{W}_k^{-1/2}\mathbf{B}_{k+1}\mathbf{W}_{k+1}^{1/2}$ *built from a cubical complex, we have*

$$\|\mathcal{L}_k^{\text{up}}\|_2 \leq \lambda_k = 2k+2.$$

Proof. From [48], the eigenvalues of the k-th renormalized *up*-Laplacian $\mathcal{L}_k^{\text{up}}$ are identical to those of the k-th *random-walk up*-Laplacian $\mathcal{L}_k^{\text{rw}} = \mathbf{W}_k^{-1}\mathbf{B}_{k+1}\mathbf{W}_{k+1}\mathbf{B}_{k+1}$. Further, let $\mathbf{L}_k^{\text{up}} = \mathbf{B}_{k+1}\mathbf{W}_{k+1}\mathbf{B}_{k+1}^\top$, following the analysis of [26], we have

$$
\begin{aligned}
\mathbf{f}^\top \mathbf{L}_k^{\text{up}}\mathbf{f} &= \left(\mathbf{W}_{k+1}^{1/2}\mathbf{B}_{k+1}^\top \mathbf{f}\right)^\top \left(\mathbf{W}_{k+1}^{1/2}\mathbf{B}_{k+1}^\top \mathbf{f}\right)\\
&= \sum_{\sigma \in K_k} \sum_{\tau \in \text{coface}(\sigma)} f^2(\sigma) w_{k+1}(\tau)\\
&\overset{\dagger}{\leq} (2k+2) \sum_{\sigma \in K_k} f^2(\sigma) \sum_{\tau \in \text{coface}(\sigma)} w_{k+1}(\tau)\\
&= (2k+2) \sum_{\sigma \in K_k} f^2(\sigma) \deg(\sigma).
\end{aligned}
$$

The inequality $\dagger$ holds using the Cauchy-Schwarz inequality; the $2k+2$ term comes from the fact that a $(k+1)$-cube has $(2k+2)$ faces. Following the rest of the proof in [26], we have

$$\|\mathcal{L}_k^{\text{up}}\| = \|\mathcal{L}_k^{\text{rw,up}}\| = \frac{\|\mathbf{L}_k^{\text{up}}\|}{\mathbf{f}^\top \mathbf{W}_k \mathbf{f}} \leq (2k+2)\frac{\sum_{\sigma \in K_k} f^2(\sigma)\deg(\sigma)}{\sum_{\sigma \in K_k} f^2(\sigma) w_k(\sigma)} = 2k+2.$$

The first equality holds due to the identical eigenvalues of $\mathcal{L}_k$ and $\mathcal{L}_k^{\text{rw}}$; the last inequality holds because we have $\mathbf{w}_k(\sigma) = |\mathbf{B}_{k+1}(\sigma)|\mathbf{w}_{k+1} = \deg(\sigma)$ for all $\sigma \in K_k$. ∎

D   Datasets, experiment details, and discussions

The edge set E of the neighborhood graph constructed using the CkNN kernel [8] is

$$E = \left\{ i,j \in V : \frac{\|\mathbf{x}_i - \mathbf{x}_j\|}{\sqrt{\rho_k(\mathbf{x}_i)\rho_k(\mathbf{x}_j)}} \leq \delta \right\}.$$

Here, $\rho_k(\mathbf{x})$ is the distance from $\mathbf{x}$ to its k-th nearest neighbor; throughout the experiment, we fix $k = 30$. The δ parameter can be chosen by a variant of the geometric consistent (GC) algorithm [29] suitable for CkNN graphs; for real datasets (except for the ocean drifter data whose geometric property is known), we use the modified GC to choose this parameter. For the rest of the datasets (synthetic manifolds and the ocean drifter), δ's are chosen manually since the topologies are known. The weights on the triangles are selected by a modification to the kernel in [12], with a similar choice of $\varepsilon = \delta^{\frac{2}{3}}/3$,

$$w_2(i,j,\ell) = \exp\left(-\frac{\|\mathbf{x}_i - \mathbf{x}_j\|^2}{\varepsilon\rho_k(\mathbf{x}_i)\rho_k(\mathbf{x}_j)}\right) \cdot \exp\left(-\frac{\|\mathbf{x}_j - \mathbf{x}_\ell\|^2}{\varepsilon\rho_k(\mathbf{x}_j)\rho_k(\mathbf{x}_\ell)}\right) \cdot \exp\left(-\frac{\|\mathbf{x}_i - \mathbf{x}_\ell\|^2}{\varepsilon\rho_k(\mathbf{x}_i)\rho_k(\mathbf{x}_\ell)}\right).$$

With this choice of parameters, the corresponding $\mathcal{L}_1$ has a large sample size limit (in terms of Δ_1) w.r.t. the metrics normalized by the k-nearest neighbor distance ρ_k.

9

D.1 Synthetic manifolds

PUNCTPLANE. PUNCTPLANE is a manifold generated by connected summing two punctured planes, with a (sparsely connected) bridge in between. Each punctured plane has a rectangular hole with width/height being $1/3$ of the width of each manifold.

TORUS. This data is a two-dimensional torus and is generated from the parameterization below,

$$
\begin{aligned}
x_1 &= (1 + 0.5\cos\theta_1)\cos\theta_2; \\
x_2 &= (1 + 0.5\cos\theta_1)\sin\theta_2; \\
x_3 &= 1 + 0.5\sin\theta_1.
\end{aligned}
$$

The sample size is $n = 1,156$. Random Gaussian noise is added on the first three dimensions as well as the additional 10 (noise) dimensions.

3-TORUS. The parameterization of 3-TORUS, a three torus with $d = 3$ and $D = 4$, is

$$
\begin{aligned}
x_1 &= (4 + (2 + \cos\theta_1)\cos\theta_2)\cos\theta_3; \\
x_2 &= (4 + (2 + \cos\theta_1)\cos\theta_2)\sin\theta_3; \\
x_3 &= (2 + \cos\theta_1)\sin\theta_2; \\
x_4 &= \sin\theta_1.
\end{aligned}
$$

We first sample $n' = 100,000$ points from this manifold; Algorithm S4 is used to generate $\mathbf{X}$ with $n = 2,000$.

GENUS-2. GENUS-2 is a two-dimensional (*genus-2*) surface generated by gluing two tori together. The implicit equation of the surface is

$$
\left(\left(x_1^2 + x_2^2\right)^2 - 0.75x_1^2 + 0.75x_2^2\right)^2 + x_3^2 = 0.01.
$$

To sample from this surface, we create a $1,000 \times 1,000$ grid in the first two coordinates (x_1, x_2) and solve for the corresponding x_3 from the above implicit equation. The aforementioned procedure generates a point cloud $\tilde{\mathbf{X}}$ ($n' \approx 551\text{k}$) having a non-uniform sampling density on the genus-2 surface; we subsample $\tilde{\mathbf{X}}$ by Algorithm S4 and obtain the final dataset $\mathbf{X}$ with $n = 1,500$.

TORI-CONCAT. TORI-CONCAT is generated by concatenating four tori together. Four tori are generated by similar procedures as TORUS with horizontal movements (in x_1) being $a = -3, 0, 3, 6$, i.e., $x_1 = (1 + 0.5\cos\theta_1)\cos\theta_2 - a$, respectively. The sample size of TORI-CONCAT is $n = 4,624$.

D.2 Real datasets

Small molecule datasets (ETH and MDA). The database [3] [13] contains several molecular dynamics (MD) trajectories, with each for a single (small) molecule, e.g., ethanol CH_3CH_2OH (ETH) and malondialdehyde $CH_2(CHO)_2$ (MDA). If a molecule has N atoms, then a point (molecular configuration) in the dataset is specified by an $N \times 3$ matrix representing the Euclidean coordinate of the configuration. To generate a point cloud from a trajectory of configurations, we first preprocess the data by calculating two angles of every triplet of atoms. Secondly, we remove the linear subspaces by keeping the top *principal components* (PCs) such that the unexplained variance ratio is less than 10^{-4}. The ambient dimensions of ETH and MDA are $D = 102$ and $D = 98$, respectively. We subsample furthest $n = 1,500$ points using Algorithm S4 for both datasets. The bond torsions (insets of Figures 3a and 3d) are calculated by the dihedral angles of the corresponding chemical bonds for each molecular configuration. For instance, the green torsion of ethanol (Figure 3a) for every point is

---

[3]Data from `http://quantum-machine.org/datasets/`

10

computed by the angle of the planes spanned by OCC and CCH in the configuration (3D Euclidean) space. One can think of the bond torsions as intrinsic coordinates of `TORUS`, i.e., θ_1 and θ_2; note that the correct bond torsions parametrizing the manifold (or $\mathbf{X}$) are usually unknown beforehand. In this work, this information is provided based on our knowledge to validate our framework.

Single-cell RNA sequencing data `PANCREAS`. `PANCREAS` [7] is a single-cell RNA sequencing data with cell cycles. The data and preprocessing codes can be found in `https://github.com/theislab/scvelo_notebooks/blob/master/Pancreas.ipynb`. The original data has sample size $n' = 3,696$; we subsample $n = 2,000$ furthest points (Algorithm S4) to remove the non-uniform sampling density on the original manifold.

3D graphics `3D-GRAPH`. The 3D model of a Buddha statue, which can be downloaded from `https://www.cc.gatech.edu/projects/large_models/`, provides a triangulation computed by [15]; in other words, the simplicial complex $\mathrm{SC}_2' = (V', E', T')$ is available beforehand, with $n' \approx 500\mathrm{k}$ and $n_1' \approx 2\mathrm{M}$. To illustrate the efficacy of our framework (and Theorem 1), we treat `3D-GRAPH` as a point cloud and build SC from the subsampled $n = 3,000$ furthest points by Algorithm S4.

Ocean buoys dataset `ISLAND`. The global Lagrangian drifter data (available in `http://www.aoml.noaa.gov/envids/gld/`) was collected by NOAA's Atlantic Oceanographic and Meteorological Laboratory and analyzed by Froyland and Padberg-Gehle [23] on the coherent flow structures of the ocean current. The dataset contains multiple trajectories of buoys dated between 2010–2019, with the location, velocity, and water temperature of each buoy recorded. The dataset itself is a 3D point cloud by converting the location (in latitude and longitude coordinates) to the *earth-centered, earth-fixed* (ECEF) coordinate system. We subsample $n = 5,000$ furthest points/buoys (Algorithm S4) with longitudes within $142°\mathrm{E}$–$179°\mathrm{E}$ and latitudes between $48°\mathrm{S}$–$33°\mathrm{S}$; namely, we sampled buoys that were located around the Tasman sea.

Medical imaging data `RETINA`. `RETINA` is one of the medical images of the STARE project [25], a retinal imaging data collection. The database consists of around 400 raw images of human retinas, with diagnosis codes, the segmented blood vessel, and the detected optic nerve available in `http://cecas.clemson.edu/~ahoover/stare/`. We use the retinal image with ID being 179, which has numerous bright (circular) spots visible. We construct the cubical complex by intensity thresholding and morphological closing, resulting in $n = 25,237$, $n_1 = 49,793$, and $n_2 = 24,548$.

D.3 Pairwise scatter plots

In this section, we show the pairwise scatter plots for $\mathbf{Z}$ (blue) and $\mathbf{Y}$ (red); specifically, we would like to show that the independent homology embedding $\mathbf{Z}$ obtained by Algorithm 1 is (approximately) factorizable. The blue embeddings (lower diagonal) in Figures S1–S6 confirm this. By contrast, most coordinate of the red embeddings $\mathbf{Y}$ do not correspond to a subspace, except for `PANCREAS` and `3D-GRAPH` in Figures S5 and S3, respectively.

11
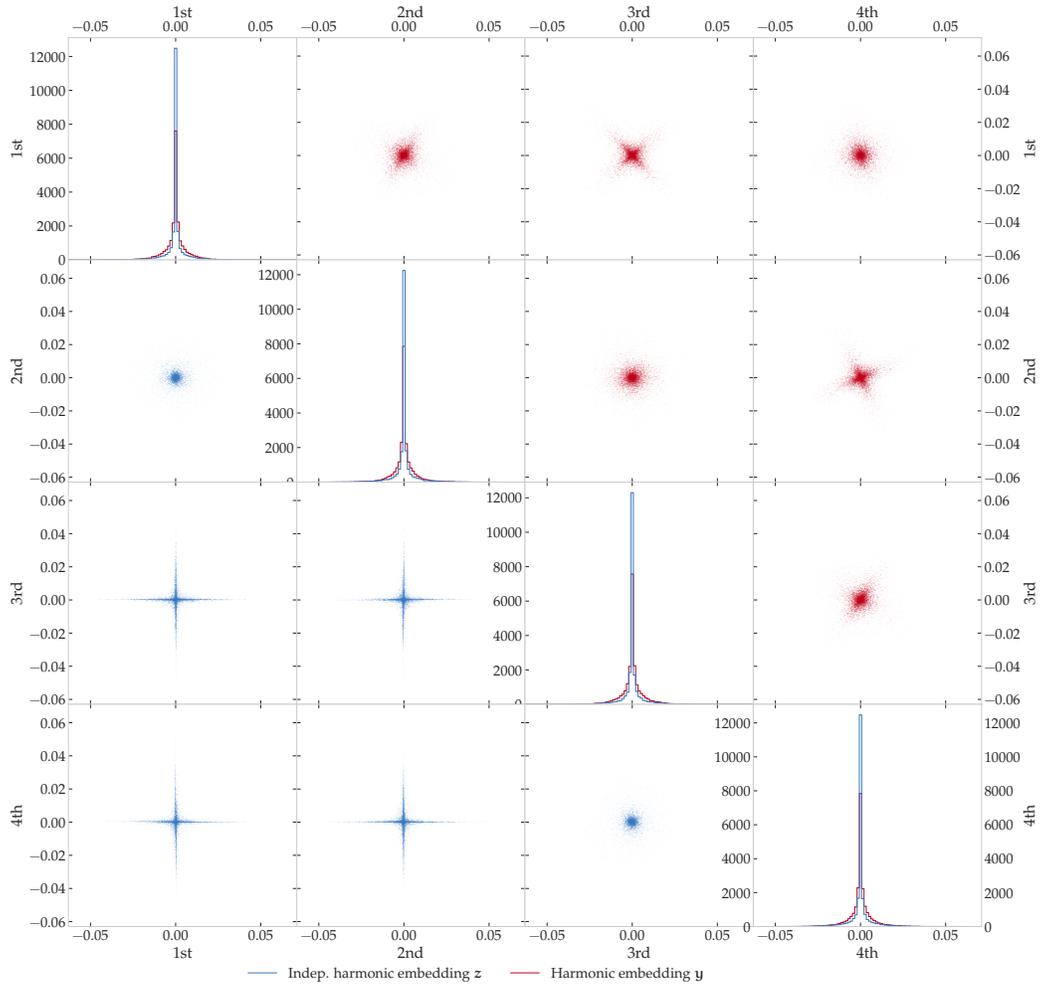
Figure S1: The independent ($\mathbf{z}$, in blue) and the coupled ($\mathbf{y}$, in red) homology embeddings of GENUS-2. The (i, j)-th (off-diagonal) subplot represents the two-dimensional scatter plot with the i-th and j-th coordinates of the embedding; the i-th diagonal term is the histograms of the i-th coordinate of the corresponding embedding.

12
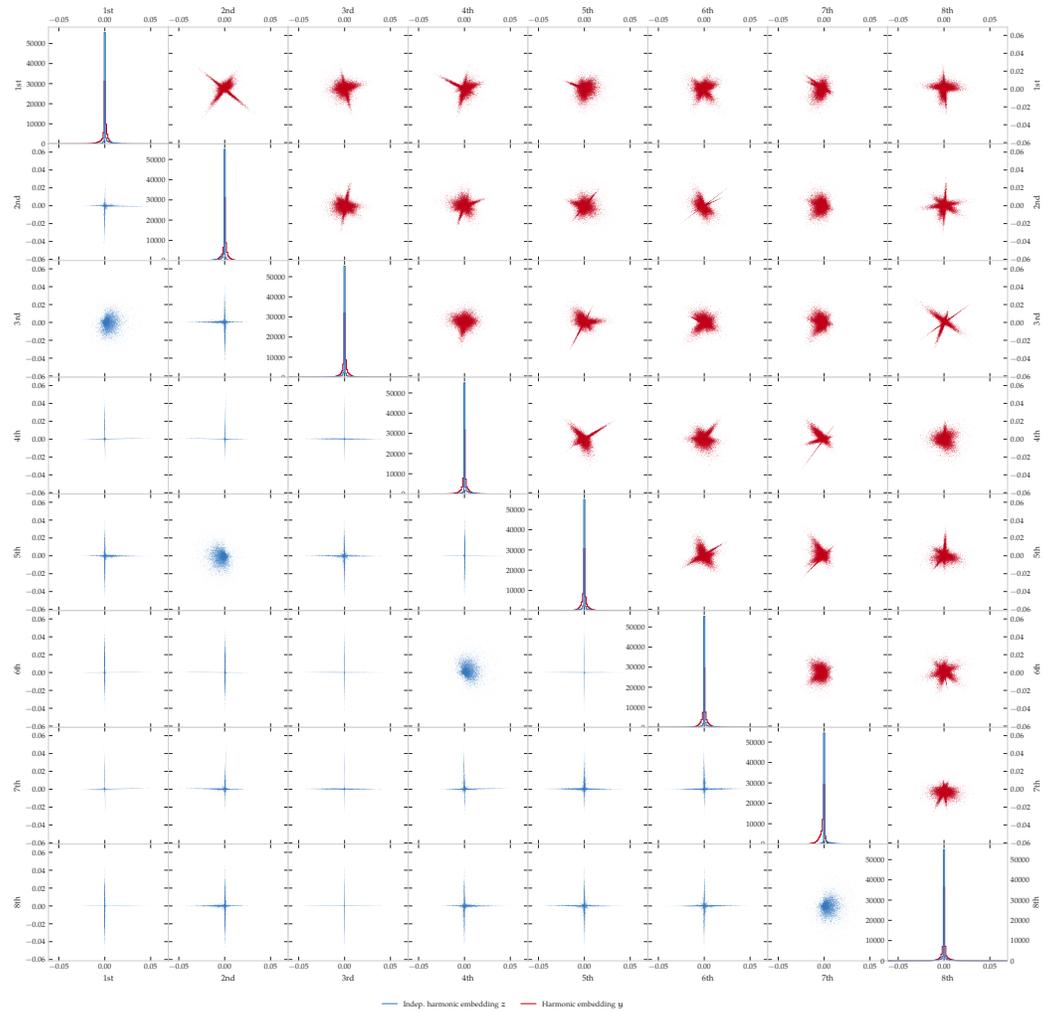
Figure S2: The independent ($\mathbf{z}$, in blue) and the coupled ($\mathbf{y}$, in red) homology embeddings of TORI-CONCAT.

13
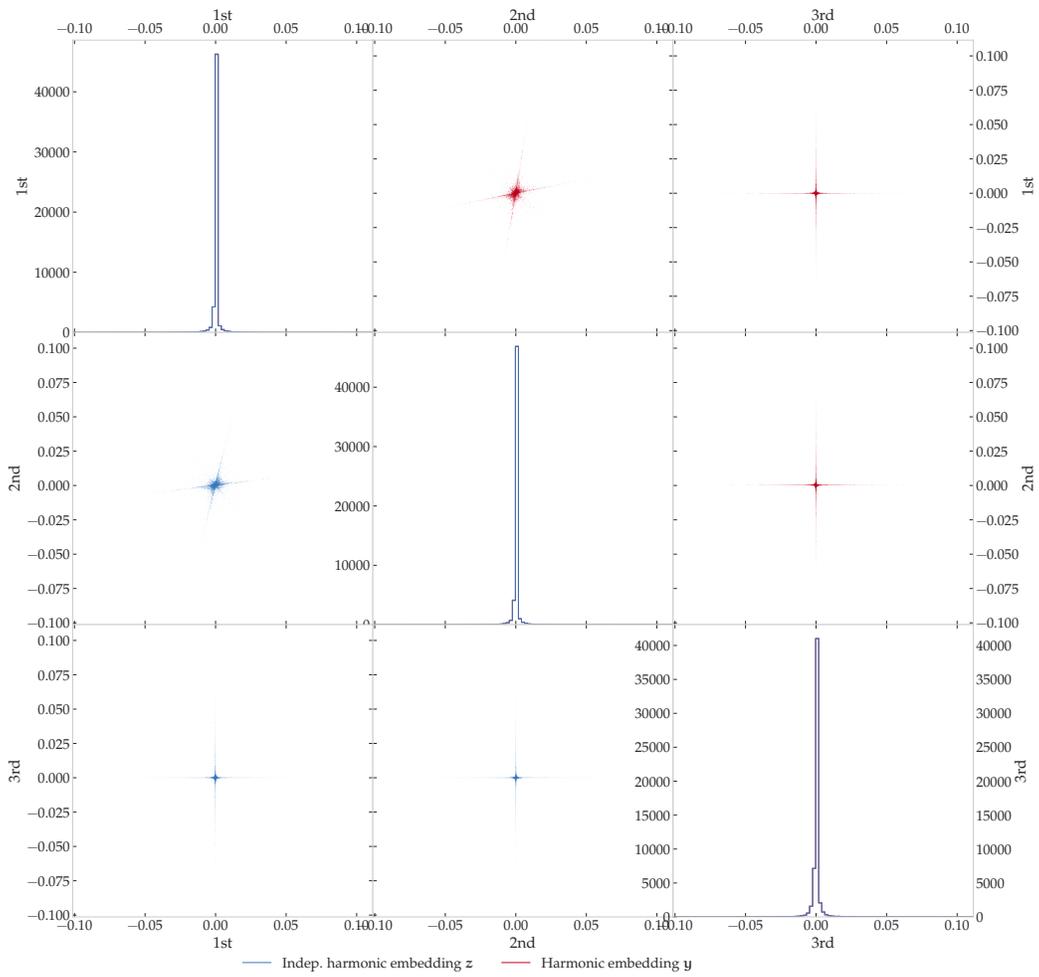
Figure S3: The independent (**z**, in blue) and the coupled (**y**, in red) homology embeddings of 3D-GRAPH.

14
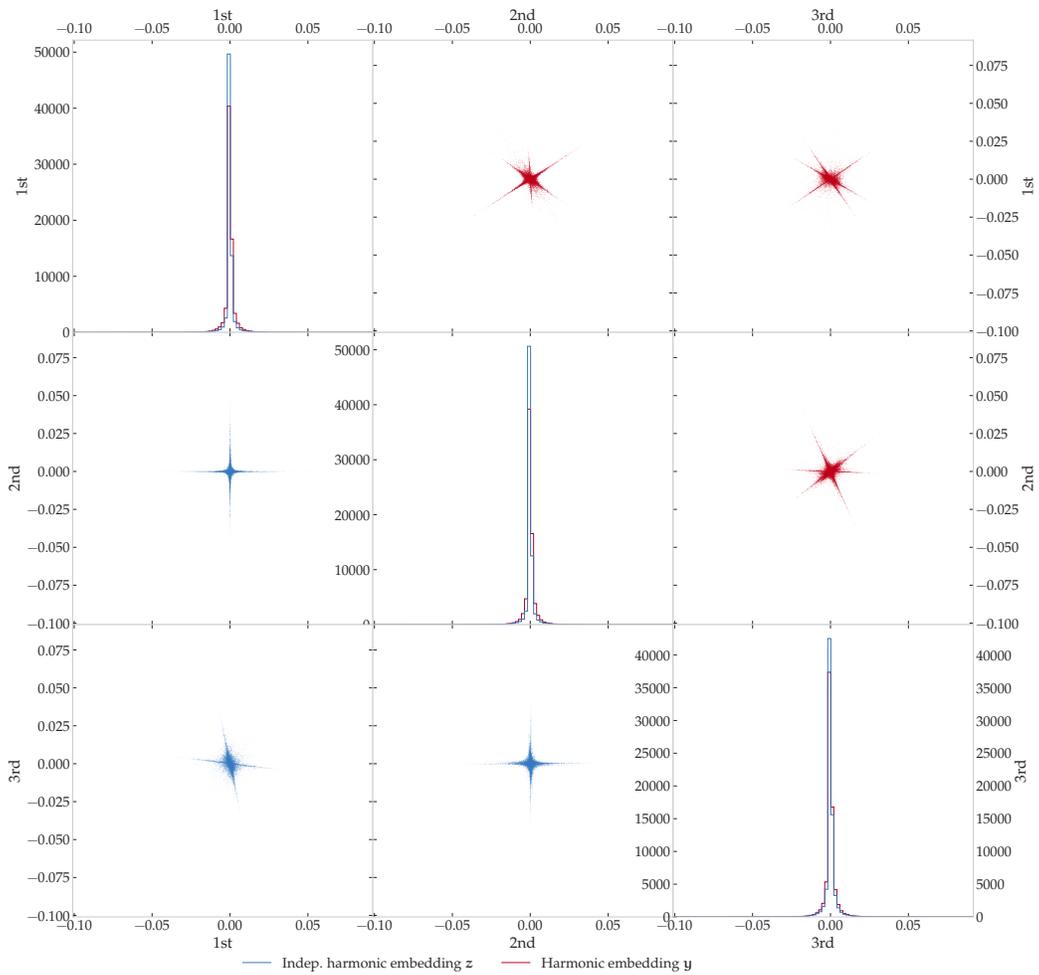
Figure S4: The independent (**z**, in blue) and the coupled (**y**, in red) homology embeddings of `ISLAND`.

15
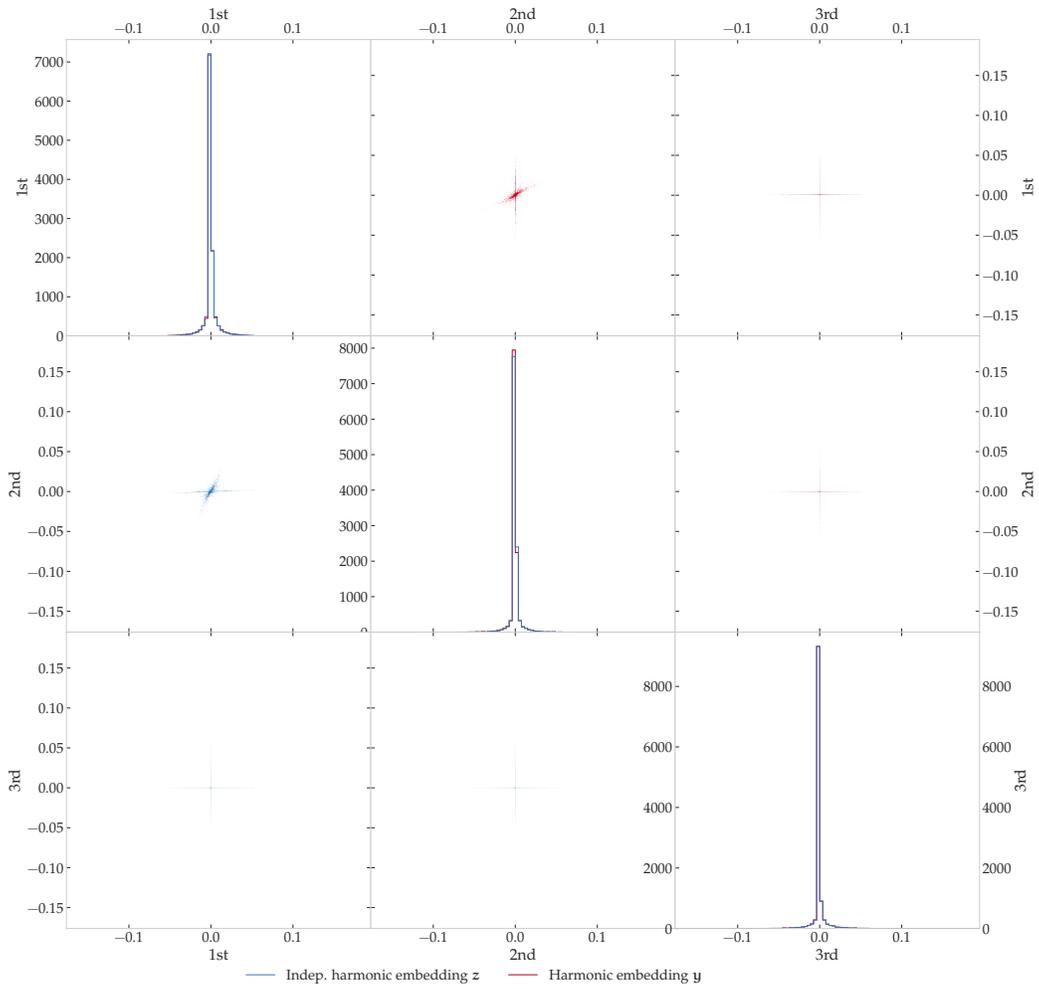
Figure S5: The independent ($\mathbf{z}$, in blue) and the coupled ($\mathbf{y}$, in red) homology embeddings of PANCREAS.

16
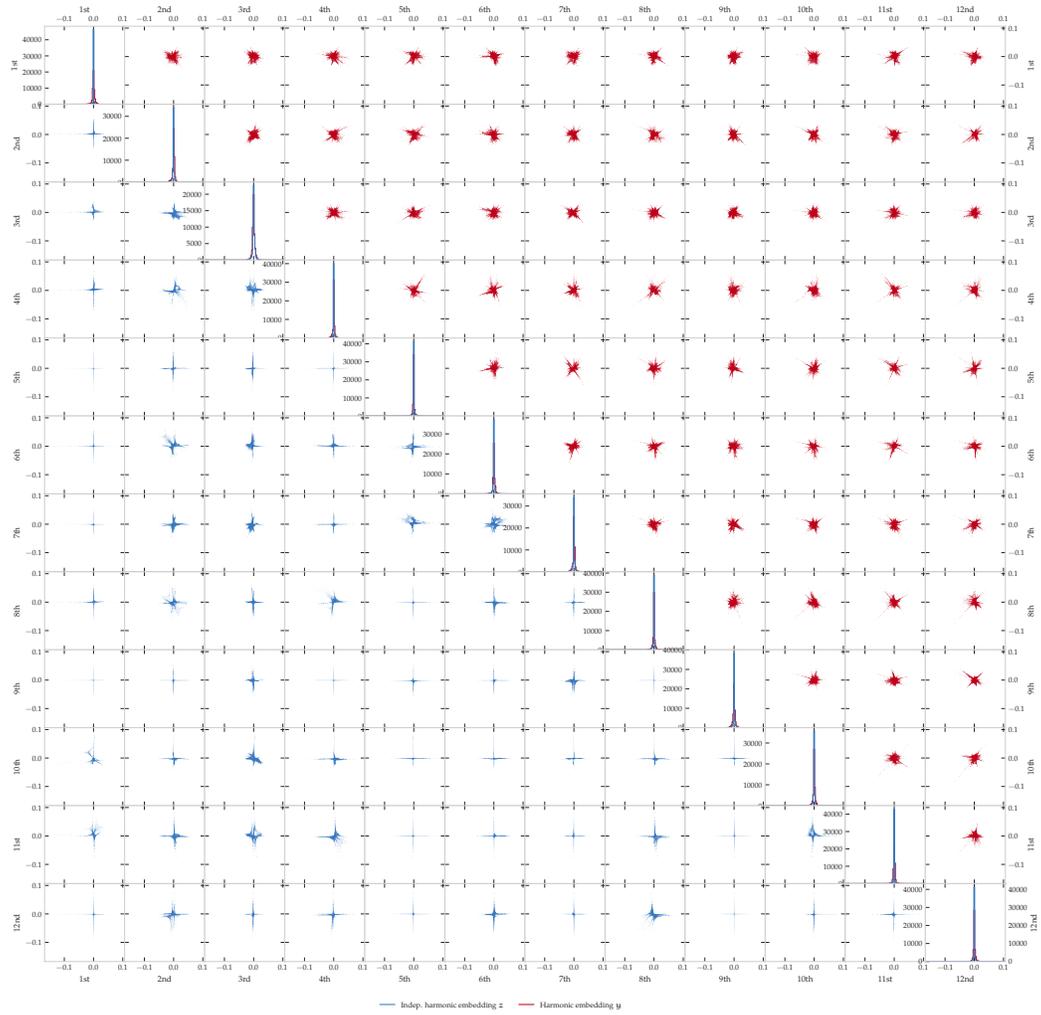
Figure S6: The independent ($\mathbf{z}$, in blue) and the coupled ($\mathbf{y}$, in red) homology embeddings of RETINA.

17
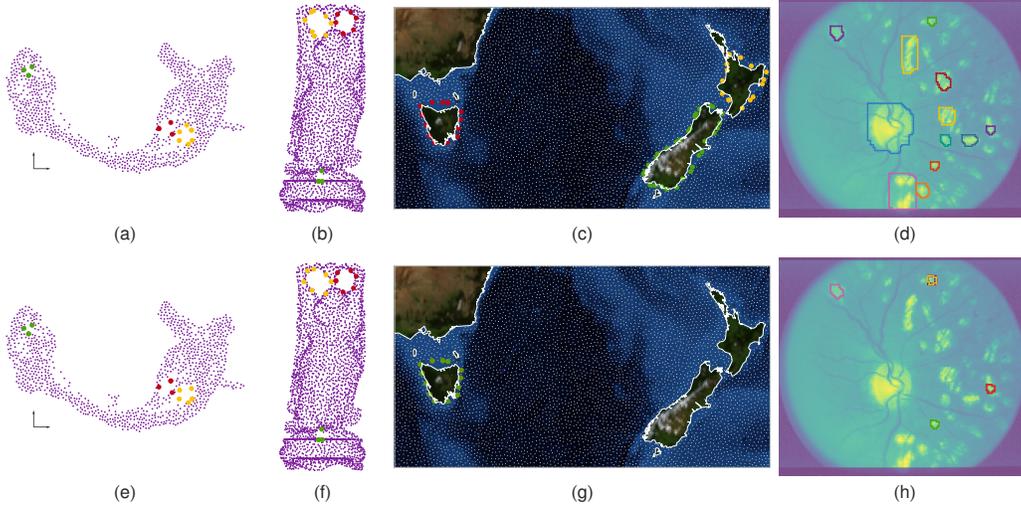
Figure S7: Comparison of the homologous loop detections on $\mathbf{Z}$ (the first row) and $\mathbf{Y}$ (the second row). The first, the second, the third, and the fourth columns present the results on PANCREAS, 3D-GRAPH, ISLAND, and RETINA, respectively. Note that (a)–(d) are identical to Figures 3g–3j.

D.4 Experiments and discussions on the shortest homologous loops detection algorithm

D.4.1 Shortest homologous loops obtained from the coupled embedding $\mathbf{Y}$

Figure S7 shows the results of the shortest homologous loop detection algorithm applied on the coupled homology embeddings $\mathbf{Y}$ on the real datasets. Note that Figures S7a–S7d are identical to Figures 3g–3j; they are presented here as comparisons to the loops detected from $\mathbf{Y}$ (the second row). As shown in Figures S7g and S7h, duplicated loops might be extracted if using the coupled embedding $\mathbf{Y}$; these loops are clearly sub-optimal.

D.4.2 Comparison to existing homologous loop detection algorithms

In this section, we discuss some existing methods in solving the problem of homologous loop detection. Some of these works offer efficient and elegant alternatives in cases when extra information is available, e.g., a triangular mesh, having an initial non-trivial loop, or in the special case of surfaces in 3D. Therefore, we see the proposed Algorithm 2, which does apply to point clouds/VR complexes with any ambient or intrinsic dimension, as complementary to these methods.

Dey et al. [17] proposed an integer programming formulation of finding the optimal homology loops given a non-trivial cycle; this problem is intrinsically different from our spectral loops extraction algorithm since no loops are given up-front. Nevertheless, the integer programming problem can be relaxed to linear programming when the boundary matrix $\mathbf{B}_2$ is total unimodular, which can be solved in $\mathcal{O}^*(\sqrt{n_1}n_2 + n_1^{5/2})$ by Lee and Sidford [34]. An example of the total unimodularity assumption to hold is when SC is constructed from a triangularization of the finite manifold. Even in this scenario, the proposed spectral loop extraction method (Algorithm 2) scales better asymptotically.

The method by Dey et al. [16] has runtime $\mathcal{O}(N^4)$, where $N = n + n_1 + n_2$ is the size of SC_2 (the detailed runtime is in the paper). By contrast, the persistent cycles extraction methods by Dey et al. [19], Wu et al. [60] use the annotation algorithm [10]. The annotation stage has a time complexity of $\mathcal{O}(N^{2.37\cdots})$. As discussed in the main paper, they are tractable for the simplicial complexes built from triangularization; however, this is not the case for VR complex since n_2 will grow fast as n increases.

Lastly, Chambers et al. [11], Dey et al. [18], Feng and Tong [22] have relatively fast runtime (in the order of $\mathcal{O}(n \log n)$). However, they either assume that the points are sampled from surfaces in 3D

18

(i.e., a genus-g surface due to the classification theorem) or the graph can be triangularized. It is oftentimes not the case for real datasets such as `ETH` or `MDA` in Figure 3.

E   Pseudocodes

Algorithm S1: Spectral homologous loop detection—an alternative to Algorithm 2

Input : $\mathbf{Z} = [\mathbf{z}_1, \cdots, \mathbf{z}_{\beta_1}]$, V, E, edge distance $\mathbf{d}$
1 **for** $i = 1, \cdots, \beta_1$ **do**
2 $\quad E_i^+ \leftarrow \{(s,t) : e = (s,t) \in E \text{ and } [\mathbf{z}_i]_e > 0\}$
3 $\quad E_i^- \leftarrow \{(t,s) : e = (s,t) \in E \text{ and } [\mathbf{z}_i]_e < 0\}$
4 $\quad E_i \leftarrow E_i^+ \cup E_i^-$
5 $\quad G_i \leftarrow (V, E_i)$, with weight of $e \in E_i$ being $[\mathbf{d}]_e$
6 $\quad e_* = (t, s_0) \leftarrow \text{argmax}_{e \in E_i} [\mathbf{z}_i]_e$
7 $\quad [s_0, s_1, \cdots, t] \leftarrow \text{DIJKSTRA}(G_i, \texttt{from=}s_0, \texttt{to=}t)$
8 $\quad \mathcal{C}_i \leftarrow [t, s_0, s_1, \cdots, t]$
Return : $\mathcal{C}_1, \cdots, \mathcal{C}_{\beta_1}$

Algorithm S2: BOUNDARYMAPS

Input : $\text{SC}_\ell = (\Sigma_0, \cdots, \Sigma_\ell)$, k
▷ Requires $\ell \geq k + 1$
1 $\mathbf{B}_k \leftarrow \text{BOUNDARYMAP}(\Sigma_{k-1}, \Sigma_k)$ ▷ Algorithm S3
2 $\mathbf{B}_k \leftarrow \text{BOUNDARYMAP}(\Sigma_k, \Sigma_{k+1})$
Return : Boundary maps $\mathbf{B}_k$, $\mathbf{B}_{k+1}$

Algorithm S3: BOUNDARYMAP

Input : Set of $(k-1)$ and k-simplices Σ_{k-1}, Σ_k (or cubes K_{k-1}, K_k)
1 $\mathbf{B}_k \leftarrow \mathbf{0}_{n_{k-1}} \mathbf{0}_{n_k}^\top \in \mathbb{R}^{n_{k-1} \times n_k}$
2 **for** *every* $\sigma_{k-1} \in \Sigma_{k-1}$ **do**
3 $\quad$ **for** *every* $\sigma_k \in \Sigma_k$ **do**
4 $\quad\quad$ **if** σ_{k-1} *is a face of* σ_k **then**
5 $\quad\quad\quad [\mathbf{B}_k]_{\sigma_{k-1}, \sigma_k} \leftarrow \text{ORIENTATION}(\sigma_{k-1}, \sigma_k)$
6 $\quad\quad$ **else**
7 $\quad\quad\quad [\mathbf{B}_k]_{\sigma_{k-1}, \sigma_k} \leftarrow 0$
Return : k-th boundary map $\mathbf{B}_k$

Algorithm S4: Furthest points sampling

Input : Initial point cloud $\tilde{\mathbf{X}} \in \mathbb{R}^{n' \times D}$, number of furthest points n
1 $\mathbf{X} \leftarrow \emptyset$
2 Pick a point $\hat{\mathbf{x}} \in \mathbb{R}^D$ randomly from $\tilde{\mathbf{X}}$
3 **for** $i = 1, \cdots, n-1$ **do**
4 $\quad \mathbf{X} \leftarrow \mathbf{X} \cup \{\hat{\mathbf{x}}\}$ ▷ Add $\hat{\mathbf{x}}$ to $\mathbf{X}$
5 $\quad \tilde{\mathbf{X}} \leftarrow \tilde{\mathbf{X}} \backslash \{\hat{\mathbf{x}}\}$ ▷ Remove $\hat{\mathbf{x}}$ from $\tilde{\mathbf{X}}$
6 $\quad \hat{\mathbf{x}} \leftarrow \text{argmax}_{\mathbf{x} \in \mathbf{X}} \min_{\tilde{\mathbf{x}} \in \tilde{\mathbf{X}}} \|\mathbf{x} - \tilde{\mathbf{x}}\|$
  $\quad$ ▷ Find the point $\hat{\mathbf{x}}$ in $\mathbf{X}$ that is furthest from $\tilde{\mathbf{X}}$
Return : Point cloud $\mathbf{X} \in \mathbb{R}^{n \times D}$

19